UNIVERSITEIT VAN PRETORIA
UNIVERSITY OF PRETORIA
YUNIBESITHI YA PRETORIA

The Mineralogy and Geochemistry of the Rooikoppies iron-rich ultramafic pegmatite body, Karee Mine, Bushveld Complex, South Africa.

By

Pieter W S K Botha

Dissertation submitted in the partial fulfilment of the

requirements for the Master of Science - (Geology)

in the Faculty of Natural and Agricultural Sciences

Department of Geology

University of Pretoria

Supervisor: Prof. R K W Merkle

March 2008

UNIVERSITEIT VAN PRETORIA
UNIVERSITY OF PRETORIA
YUNIBESITHI YA PRETORIA

Intellection Pty Ltd,

27 Mayneview Street,

Milton,

Queensland, 4064, Australia

UNIVERSITEIT VAN PRETORIA
UNIVERSITY OF PRETORIA
YUNIBESITHI YA PRETORIA

The Mineralogy and Geochemistry of the Rooikoppies iron-rich ultramafic pegmatite body, Karee Mine, Bushveld Complex, South Africa.

By

Pieter W S K Botha

Dissertation submitted in the partial fulfilment of the

requirements for the Master of Science - (Geology)

in the Faculty of Natural and Agricultural Sciences

Department of Geology

University of Pretoria

Supervisor: Prof. R K W Merkle

March 2008

The Mineralogy and Geochemistry of the Rooikoppies iron-rich ultramafic pegmatite body, Karee Mine, Bushveld Complex, South Africa.

Pieter W.S.K. Botha[*] and Roland K.W. Merkle[#]

*Intellection Pty Ltd, 27 Mayneview Street, Milton, Queensland, 4064, Australia

[#]Department of Geology, University of Pretoria, Pretoria 0002, South Africa

Key Words: Bushveld Igneous Complex; Iron-rich Ultramafic Pegmatite; Hydrous Replacement; Alteration; Rustenburg Layered Suite; Upper Critical Zone.

Abstract

At the Karee Mine of the Lonplats mining company in the Bushveld Complex, South Africa, the Rooikoppies iron-rich ultramafic pegmatite (IRUP), which covers the stratigraphy from below the UG2 chromitite layer up to the Main Zone, replaces cumulus anorthosite and pyroxenite.

The Rooikoppies IRUP was studied using transmitted and reflected light microscopy, X-ray fluorescence, X-ray diffraction, and electron microprobe techniques. Two visually different varieties of IRUP were observed: a) a relatively smaller grained greyish variety and b) a relatively coarser grained greenish variety. In drill core, the IRUP body was observed to be in contact with the host cumulate rocks either by means of gradual or sharp contacts. Bulk rock compositions indicate that the Rooikoppies IRUP is enriched in Fe_2O_3, MgO, and CaO (relative to the cumulate host rocks) while having lower concentrations of Al_2O_3. Chemical differences between cumulus host rocks and IRUP are accompanied by changes in mineral assemblage and mineral chemistry. Spatially related IRUP samples revealed areas with potentially more pronounced increases in iron and magnesium contents relative to the host cumulate rocks.

Element ratios indicate that aluminium acted as an immobile element during the formation of the IRUP body and that the addition of iron, magnesium, and calcium, through the action of hydrothermal fluids, diluted the already existing cumulus feldspar, resulting in the low concentrations of Al_2O_3 in the IRUP samples. The addition of iron, magnesium, and calcium also resulted in the crystallization of large proportions of clinopyroxene and olivine, and resulted in changes in the mineral assemblage and mineral chemistry, relative to the host cumulate rocks. The Rooikoppies IRUP body can be classified as a silicate rich variety (Viljoen and Scoon, 1985), consisting of clinopyroxene, olivine, plagioclase, secondary magnetite and ilmenite. It is suggested that the formation of the Rooikoppies IRUP is not due to a single event, but rather that the IRUP body formed through multiple replacement events, resulting in a network of chemically different zones within one large IRUP body.

Introduction

The Bushveld Igneous Complex (BIC) is a large layered magmatic intrusion situated in the north-eastern parts of South Africa. In many areas of the BIC, post cumulus ultramafic rocks crosscut the igneous layering of the Rustenburg Layered Suite (RLS), including the UG2 chromitite layer and the Merensky Reef. These post cumulus rocks have received the nomenclature of "ultramafic pegmatite", which, according to Viljoen and Scoon (1985), distinguishes their post cumulus transgressive nature, and coarse grain size from the term "pegmatoid", commonly used in the Bushveld literature to indicate the textures of concordant cumulate rocks. The compositions of ultramafic pegmatites are greatly variable throughout the Bushveld Complex; therefore, Viljoen and Scoon (1985) developed a broad classification scheme based on the mineralogical and chemical characteristics of these rocks. The scheme classifies the ultramafic bodies into three main groups:

1) Iron rich ultramafic pegmatite (IRUP)
   a) A silicate rich variety:
      Consists mainly of olivine and clinopyroxene, and lesser Fe-Ti oxides.
   b) A Fe-Ti oxide variety:
      Consists mainly of Fe-Ti oxides.
2) Non-platiniferous magnesian dunite, and
3) Platiniferous ultramafic pipes.

The area of this study is located in the western lobe of the Bushveld Complex, towards the east of Rustenburg, in the Marikana area, at the Karee mine of the Lonplats mining company. At this location, the Rooikoppies ultramafic pegmatite (Figure 1) has been intersected in drill core to a depth of 700 m. In the available drill cores, the Rooikoppies IRUP covers the stratigraphy from below the UG2 chromitite layer up into the Main Zone.

Ultramafic pegmatite samples were described in terms of their mineralogy and petrographic characteristics in order to accurately classify the Rooikoppies pegmatite into one of the groups suggested by Viljoen and Scoon (1985).

Investigation into the reflection of original cumulate compositions in IRUP was conducted by studying samples from equal stratigraphic levels in two adjacent boreholes (R14 and R112, which were both sampled for IRUP and original cumulate rock). In the upper critical zone, IRUP replaces both the footwall anorthosite and hanging wall pyroxenite layers of the UG2 chromitite. IRUP samples were collected from above and below the UG2 chromitite to investigate whether the difference in original cumulate mineralogy resulted in a difference in the mineralogical and geochemical composition of IRUP. In boreholes R151 and R14 mottled anorthosite and spotted anorthosite, respectively, appears to become progressively replaced by IRUP. These samples provide the opportunity to document the geochemical and mineralogical changes from an unreplaced to totally replaced rock along samples of 3.03 m and 1.25 m in length respectively. In addition to examining the geochemistry and mineralogy of these visually gradational contact (VGC) zones between IRUP and

host cumulate rock, the results of mineral chemistry studies (by Electron Microprobe Analysis) on VGC's provided even more detail with regard to the chemical changes involved with the formation of IRUP bodies.

A critical aspect involved in the formation of IRUP is the nature of the fluid ("fluid" referring to any low viscosity medium with the ability to infiltrate and replace cumulate rocks, be it an aqueous solution or a melt) responsible for the replacement of cumulate rocks. The geochemical data collected in this study provide additional information to assist in formulating hypotheses as to the chemical composition and nature of the IRUP-forming fluid.

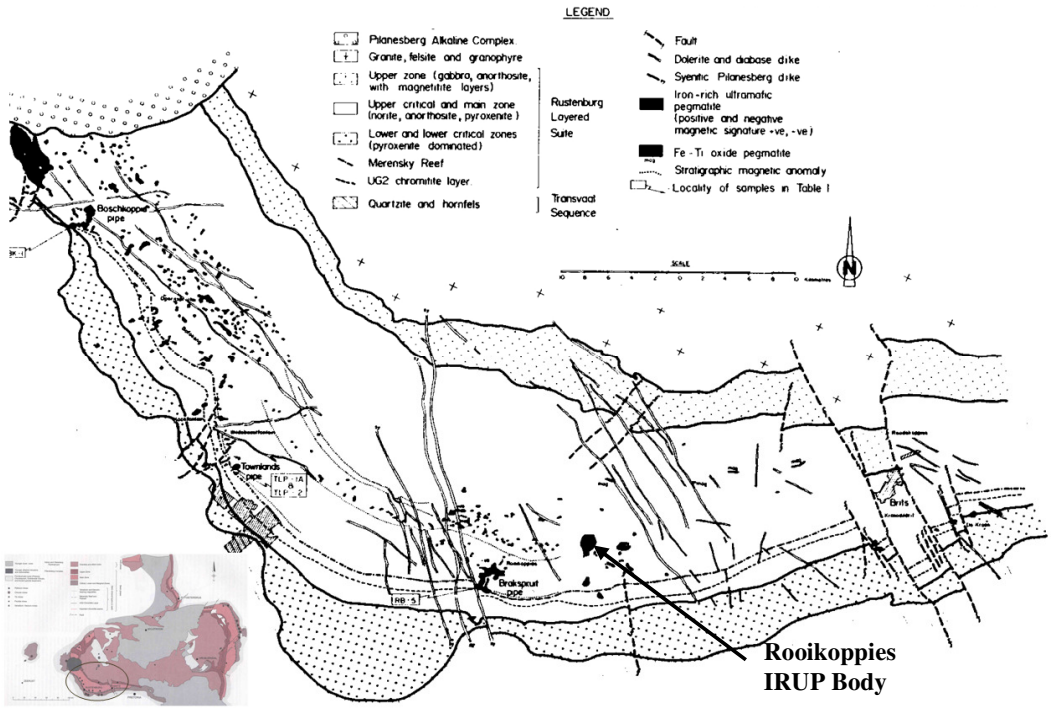

Figure 1: The distribution of ultramafic pegmatite bodies in a part of the western Bushveld Igneous Complex (Viljoen and Scoon, 1985 and Wilson and Anauesser, 1998).

This study focuses on an IRUP body in non-mineralized layers of the Upper Critical Zone in the RLS. It must be emphasised that the purpose of this study is not to establish above all doubt what the physical mechanism of replacement was, but rather to understand the bulk geochemistry of the IRUP, what its mineralogical composition is, and the variation of the mineral chemistry. Such descriptions will provide the opportunity for comparison between IRUP bodies, which may highlight similarities or differences in terms of the processes of formation. Studying the effects of IRUP formation processes on economic horizons, such as the UG2 chromitite layer or the Merensky Reef, falls outside the scope of this study.

Sampling:

Three boreholes were selected for sampling:

a) Borehole R14,
b) Borehole R151, and
c) Borehole R112.

The locations of these drill cores are illustrated in Figure 2. Drill cores R14 and R112 were selected because of their intersection with the UG2 chromitite layer, which made it possible to correlate the igneous layering in the two drill cores. A third drill core, R151, displayed three areas of replacement where the host rock is in gradual contact with IRUP. As drill cores R14 and R112 contain the highest amount of IRUP and were logged from top to bottom (core logs are included as Appendix A). Drill core R151, however, was only described in terms of the replacement material and host rock sampled. A description of samples and why they were collected follows in Chapter 4.2.2. The three main rock types found in the drill core are: spotted anorthosite (leuconorite), mottled anorthosite, and IRUP.

Spotted anorthosite (leuco-norite) – described as an anorthositic rock containing mainly plagioclase with "spots" of pyroxene. The "spots" of pyroxene measure approximately 2.5 – 5 mm in diameter and appear to be randomly distributed throughout the rock.

Mottled anorthosite (leuco norite) – described as an anorthositic rock containing mainly plagioclase with "mottles" of pyroxene. The "mottles" of pyroxene measure approximately 2 – 3 cm in diameter and appear to be distributed randomly throughout the rock.

IRUP occurs in two visually different varieties. A greenish variety that appears to be slightly coarser grained, with an average grain size of approximately 3.3 cm. The other variety of IRUP has a greyish colour, and an average grain size of approximately 1.8 cm. Both varieties of IRUP display variable degrees of magnetism in borehole R14 and R112. In terms of distribution in the drill cores, the two IRUP varieties appear to be randomly distributed throughout drill core R112, while below a depth of 544 m, in drill core R14, the grey variety is more abundant, whereas, above 544 m, the greenish variety appears more frequently.

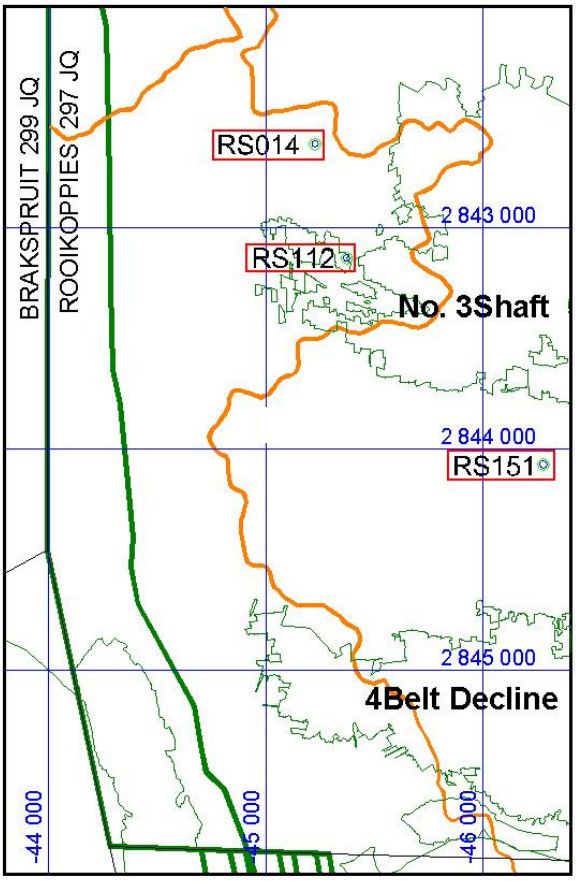

Figure 2: A plan map of the locations of drill cores R14, R151, and R112.

Samples were collected to investigate the following aspects of IRUP:

1) The nature of gradual contacts between IRUP and host rock,
2) The Geochemical differences between visually different IRUP,
3) Comparison between replaced and unreplaced rock,
4) The replacement of host rock above and below the UG2 chromitite layer, and
5) The composition of IRUP at variable stratigraphic levels.

1) Based on the visual changes along several lengths of drill core, it appears as if some original cumulate rock was progressively replaced by IRUP. These visual changes essentially represent gradual contacts between IRUP and their host rocks (Figure 2.1). For the study of the possible "progressive replacement process", two lengths of drill core – both displaying gradual contacts between IRUP and host rock – were selected: one length from borehole R151 and one length from borehole R14. The samples provided the opportunity to study the changes in the whole rock chemistry, mineralogy, and mineral chemistry associated with the formation of IRUP.

Figure 2.1: An example image of a gradational contact between host rock (image illustrates mottled anorthosite) and IRUP.

a) Length of drill core from borehole R151 (i: samples 1-18):
   i) Mottled anorthosite (leuco norite) is in gradual contact with IRUP. Unreplaced leuco-norite is located at the lower end of the sample, while IRUP is located at the upper end (Figure 2.2). This length of drill core will be referred to as "MAR" – Mottled Anorthosite Replacement.

b) Length of drill core from borehole R14 (samples 19-26):
   i) Spotted anorthosite (leuco-norite) is in gradual contact with IRUP. Unreplaced spotted anorthosite is located at the lower end of the sample, while IRUP is located at the upper end (Figure 2.3). This length of Drill core will be referred to as "SAR" – Spotted Anorthosite Replacement.

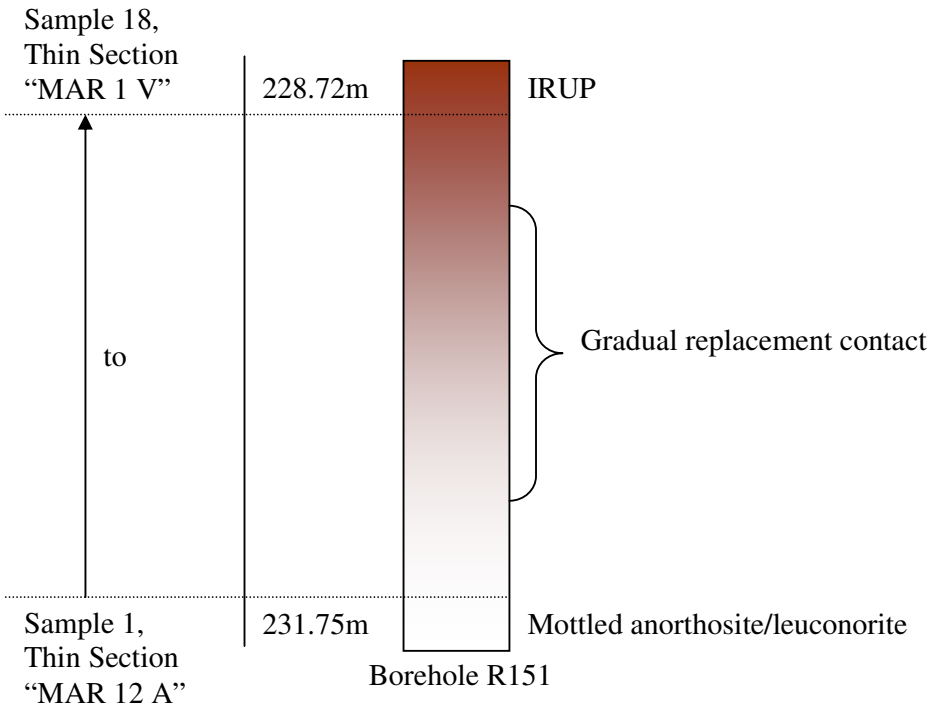

Figure 2.2: The gradual replacement contact between IRUP and unreplaced mottled anorthosite. The length of drill core is referred to as "MAR". This image does not represent the entire length of sampled drill core.

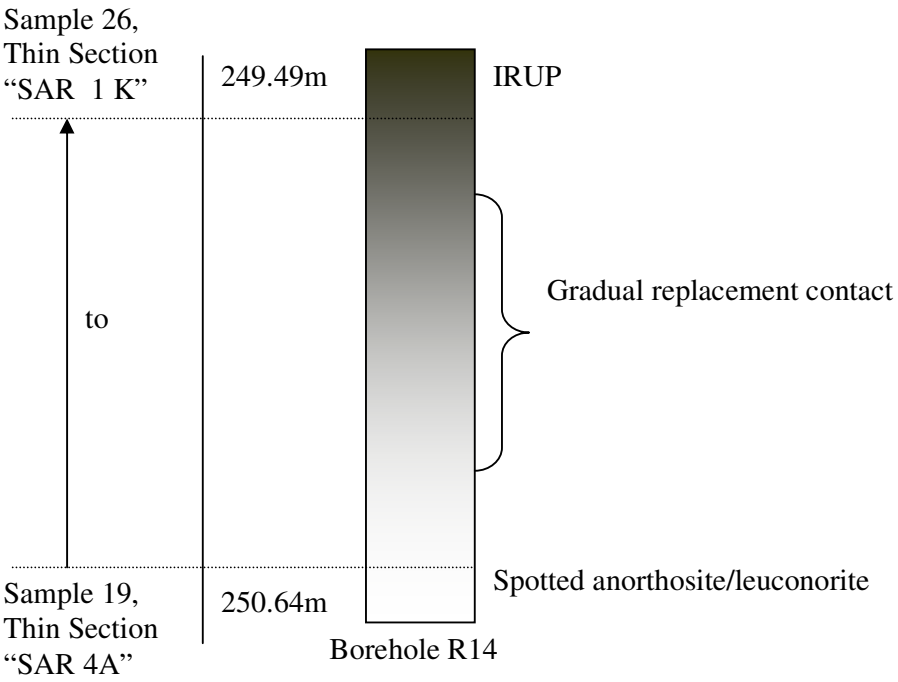

Figure 2.3: The gradual replacement contact between IRUP and unreplaced spotted anorthosite. The length of drill core is referred to as "SAR".

2) In addition to the gradual contacts, some lengths of drill core contain sharp contacts between IRUP and anorthosite. Two samples, one containing a sharp contact between the relatively smaller grained greyish variety of IRUP and spotted anorthosite, and one with a sharp contact between the coarser grained greenish variety of IRUP and mottled anorthosite, were collected from borehole R14 and R112 respectively to study the whole rock geochemical differences between the two varieties of IRUP (Figure 2.4 a and b). The host cumulate rocks and the IRUP were separated at the contact and analysed separately.

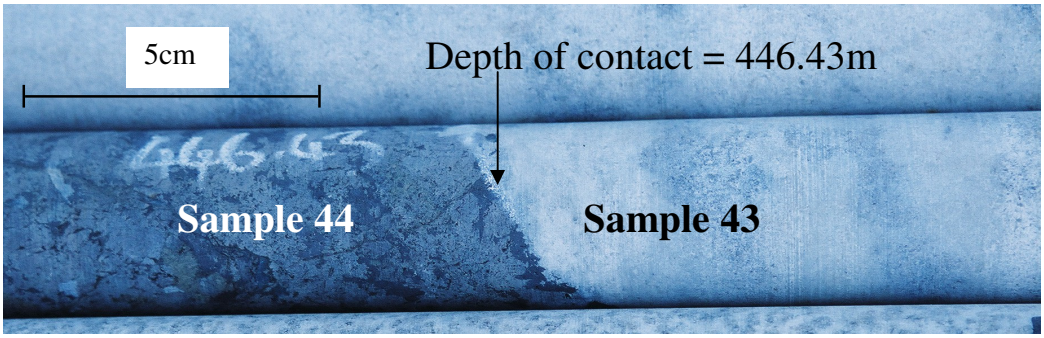

Figure 2.4 a: The sharp contact between IRUP (coarser grained greenish variety) and unreplaced mottled anorthosite (sample 43 and 44 at approximately 446.43 m in borehole R112).

Figure 2.4 b: The sharp contact between IRUP (smaller grained greyish variety) and unreplaced spotted anorthosite (sample 45 and 46 at approximately 665 m in borehole R14).

3) IRUP samples from borehole R112 were collected for comparison with unreplaced cumulate rock samples from borehole R14 at equivalent stratigraphic levels. Similarly, IRUP samples from borehole R14 were collected for comparison with unreplaced cumulate rock samples from borehole R112 at equivalent stratigraphic levels (Figure 2.5). These samples may also assist in establishing whether or not any chemical, physical, or mineralogical features of the original cumulate rocks are retained in the IRUP. Furthermore, the samples enable the consideration of what the influence of the composition of the original cumulate rock is on the composition of IRUP.

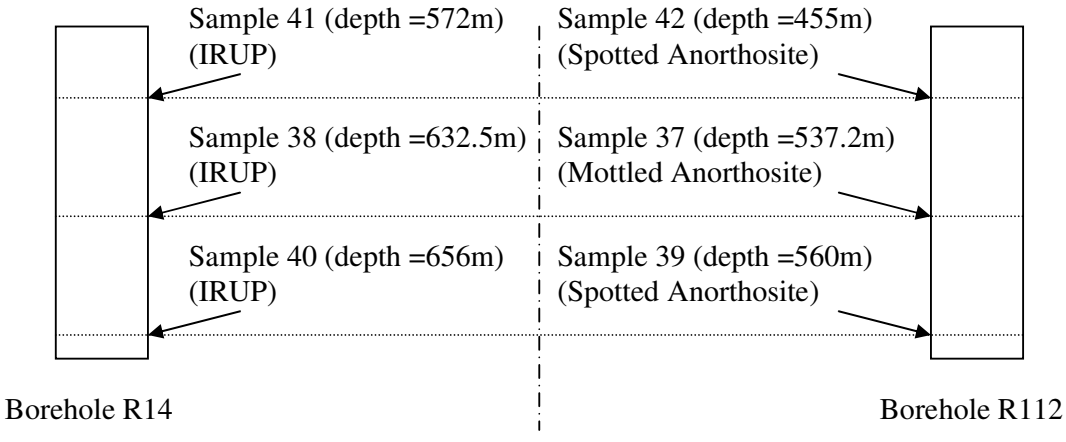

Figure 2.5: The positions of samples for comparison in boreholes R14 and R112. Samples were collected at roughly equal stratigraphic levels (not to scale).

4) Borehole R14 intersects the UG2 chromitite layer, which is an accurate indication of stratigraphic height. IRUP replaces both the footwall anorthosite and hanging wall pyroxenite layers of the UG2 chromitite. IRUP samples were collected from above and below the UG2 chromitite (with accurate indications of their stratigraphic level) to investigate whether the difference in original cumulate mineralogy resulted in a difference in the mineralogical and geochemical composition of IRUP (Figure 2.6).

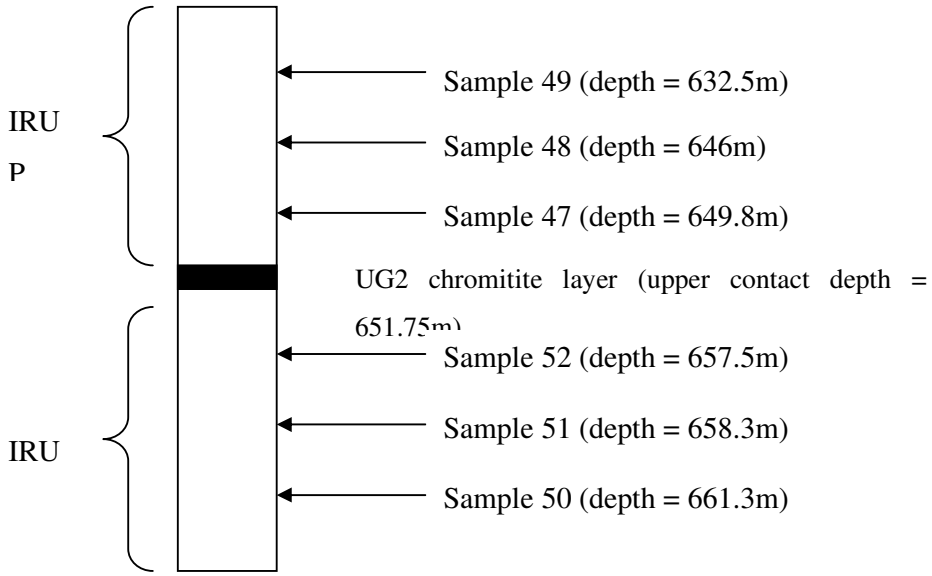

Figure 2.6: Sampling depths above and below the UG2 in borehole R14 (not to scale).

5) Samples were collected at different stratigraphic levels in borehole R14 to investigate whether or not the composition of IRUP changes with stratigraphic height. The samples of pure IRUP (samples number 23 (249.96 m), 24 (249.79 m), 25 (249.65 m), and 26 (249.54 m)) in sample "SAR" from borehole R14 (Figure 4.7) will be compared with IRUP samples number 41 (572m), 38 (632.5m) and 40 (656m) – Figure 2.5 – from borehole R14.

Petrography

Mottled Anorthosite:

Mottled anorthosite consists of approximately 70% - 80% plagioclase and 20% - 30% pyroxene. Accessory phases may include olivine, which generally does not occur in quantities of more than 5%, chromite, and secondary magnetite. The mottled anorthosite hosts almost no oxides or sulphides, is medium to coarse grained (0.5mm to 1mm grain size), and exhibits a granular texture.

Plagioclase in mottled anorthosite is of cumulus origin and is generally subhedral, with well-oriented and fairly parallel polysynthetic twinning (Figure 3.1). A limited amount of alteration of plagioclase occurs in the form of saussuritization. There

appears to be no difference in the degree of alteration of plagioclase in the samples that display gradual contacts between host rock and IRUP, whether the plagioclase is far from, or close to, the contact between IRUP and mottled anorthosite.

Mottled anorthosite contains mostly clinopyroxene with lesser amounts of orthopyroxene (less than 5%). Anhedral clino- and orthopyroxene exists as interstitial phases between cumulus plagioclase grains, with many grains of clinopyroxene containing orthopyroxene exsolution lamellae. In some thin sections, large grains of clinopyroxene have anhedral inclusions of plagioclase (Figure 3.2). In addition to their interstitial relationship with plagioclase, pyroxene grains form oikocrysts, which poikilitically enclose subhedral plagioclase. Pyroxene displays "patchy" alteration to a light green mineral that displays pleochroism and first order brown interference colours, which was identified as amphibole (ranging in composition from hornblende to actinolite).

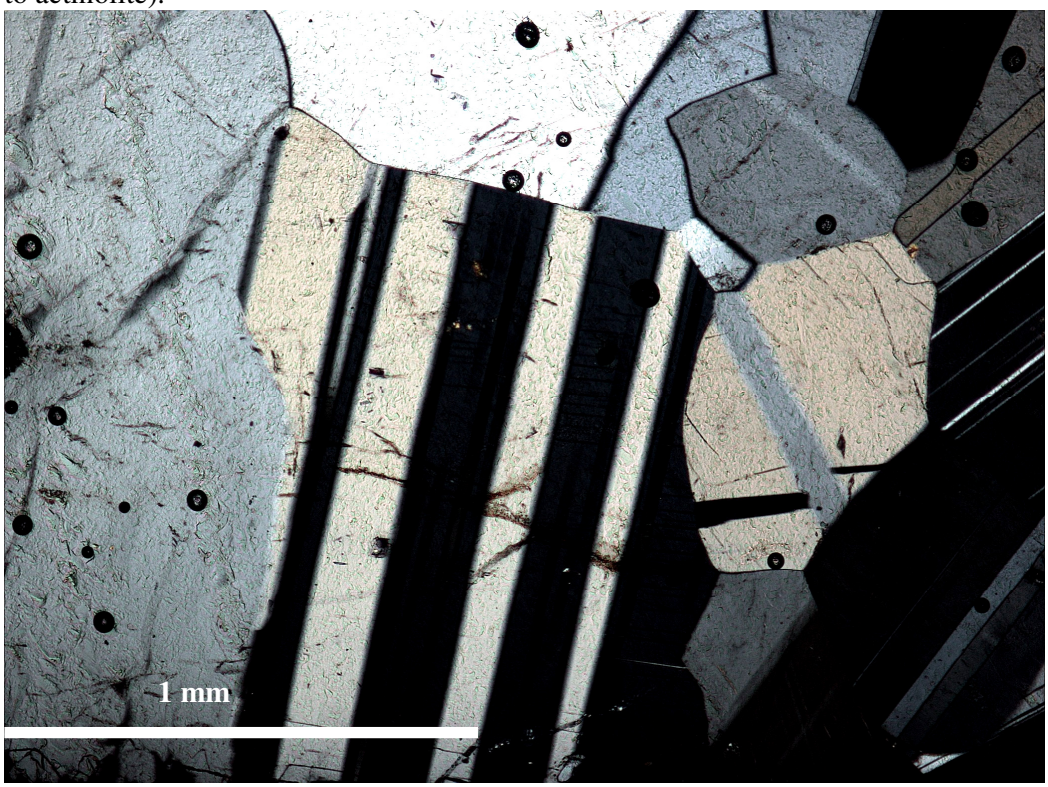

Figure 3.1: The nearly parallel polysynthetic twinning of a subhedral, first generation plagioclase grain (thin section MAR 12B). Crossed polars.

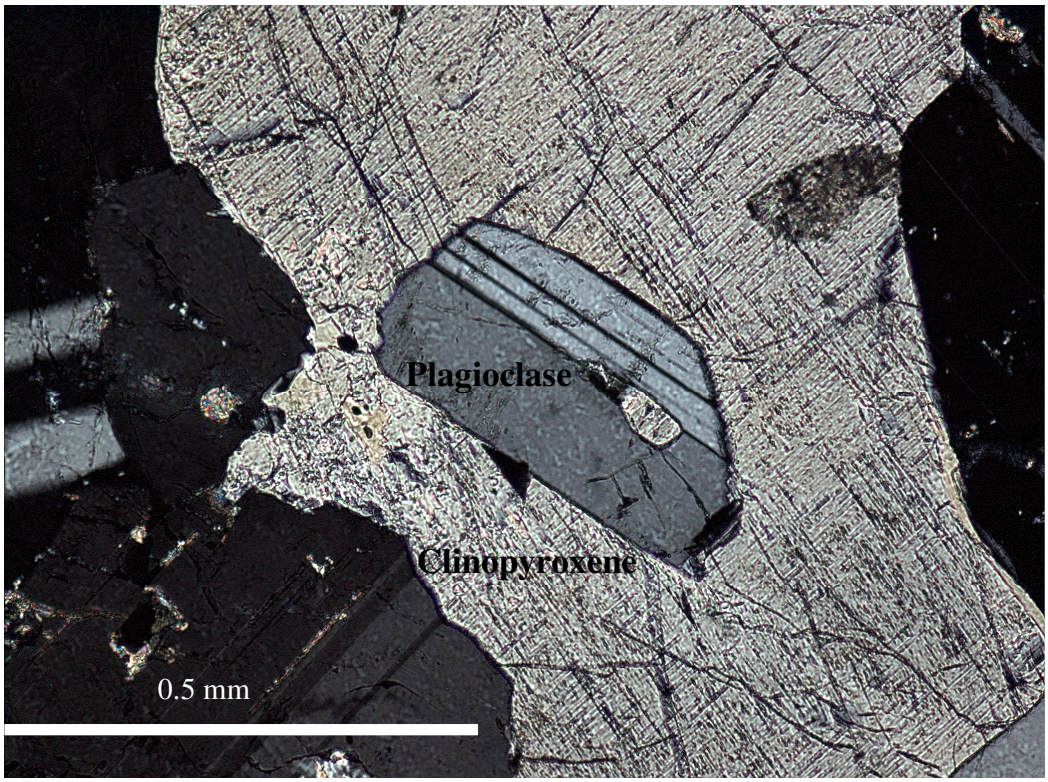

Figure 3.2: A large clinopyroxene grain with an inclusion of plagioclase (thin section MAR 9H). Crossed polars.

Clinopyroxene appears to have a constant degree of alteration in almost all thin sections of mottled anorthosite; however, one thin section contains an anomalously large pyroxene grain, with augitic twinning, and a high degree of alteration to amphibole (Figure 3.3).

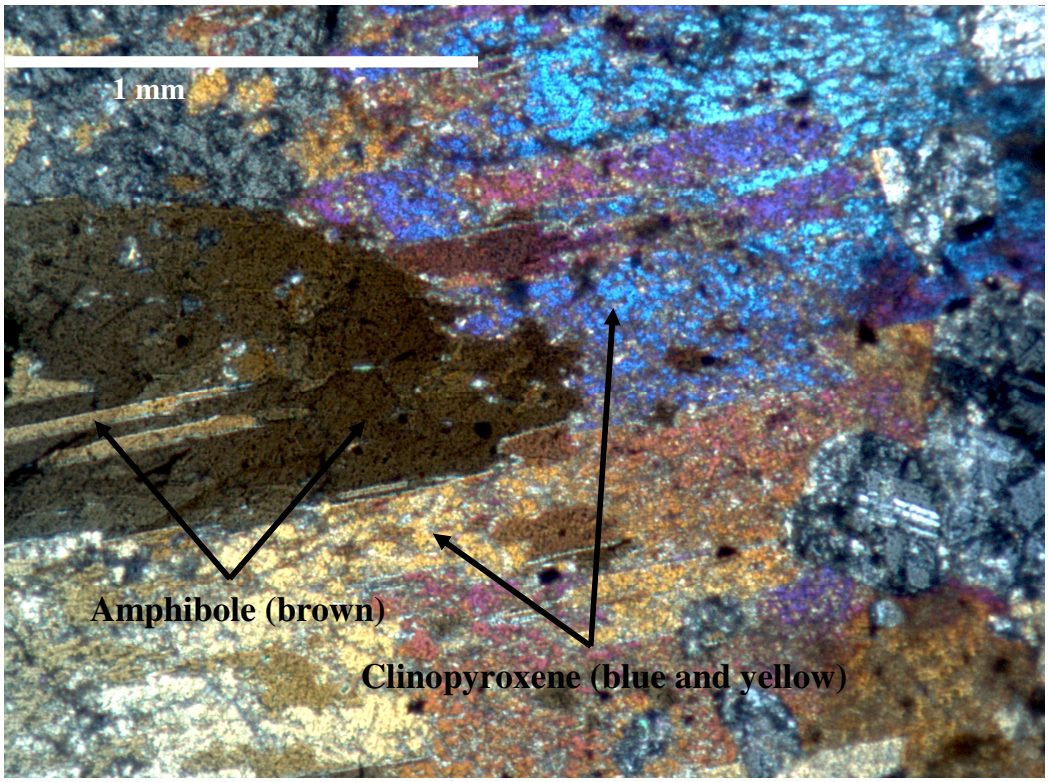

Figure 3.3: A large clinopyroxene grain, displaying augitic twinning, with intense alteration to amphibole (thin section MAR 9G). Crossed polars.

Olivine is mostly anhedral, and displays its characteristic alteration to serpentine, with associated magnetite, which forms due to the oxidation of Fe^{2+} to Fe^{3+} during serpentinization, along irregular oriented cracks and at grain boundaries.

Spotted Anorthosite:

The spotted anorthosite consists of approximately 80% - 90% plagioclase and 10% - 20% pyroxene. Olivine is generally a minor phase occurring in amounts less than 5%. Spotted anorthosite is medium to coarse grained (0.5mm to 1mm grain size) and displays a granular texture.

Similar to the mottled anorthosite, plagioclase from the spotted anorthosite is subhedral to euhedral, and of cumulus origin. The main form of alteration is saussuritization, which occurs in limited amounts. In the samples that display gradual contacts between host rock and IRUP, the degree of alteration of plagioclase seems constant in all thin sections, whether the plagioclase is far from, or close to, the contact between IRUP and spotted anorthosite.

Pyroxene is dominated by clinopyroxene, which has an interstitial relationship to plagioclase. Some clinopyroxene grains are distinctively large, display uncharacteristic first order grey interference colours, contain finely spaced exsolutions of orthopyroxene, and have inclusions of plagioclase grains (Figure 4).

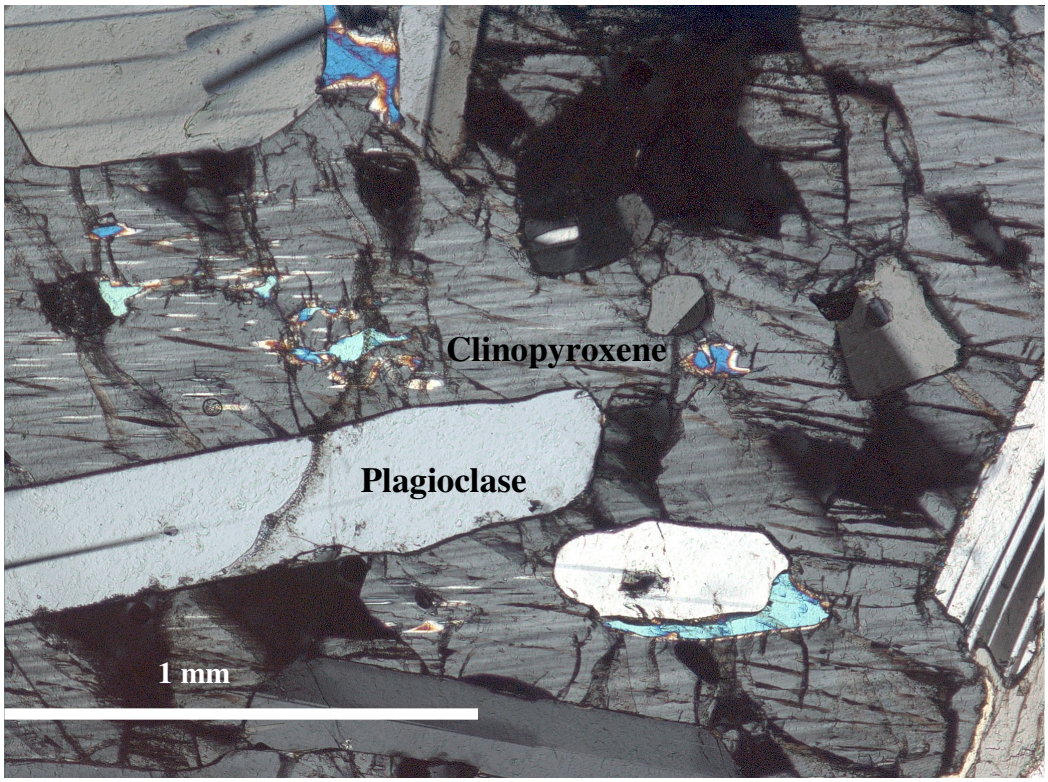

Figure 4: A large clinopyroxene grain with finely spaced exsolution lamellae and inclusion of anhedral to subhedral plagioclase grains (thin section SAR 4A). Crossed polars.

IRUP:

IRUP mainly consists of clinopyroxene and olivine, with lesser amounts of plagioclase consistently present. Oxides and sulphides appear more frequently in the form of magnetite, ilmenite, pyrrhotite and pentlandite. The IRUP is a coarse grained rock, with olivine and clinopyroxene grains measuring up to 3 cm in diameter. Thin sections frequently host only one or two large grains of pyroxene and olivine; therefore, the rock textures could not always be evaluated.

Clinopyroxene is euhedral, displays augitic twinning, and variable degrees of "patchy" alteration to amphibole – visually estimated up to 10%, and ranging in composition from hornblende to actinolite. Grains of magnetite frequently accompany the alteration of pyroxene to amphibole. Figure 5.1 illustrates a twinned clinopyroxene in IRUP, the "patchy" alteration of pyroxene to amphibole, and some grains of magnetite.

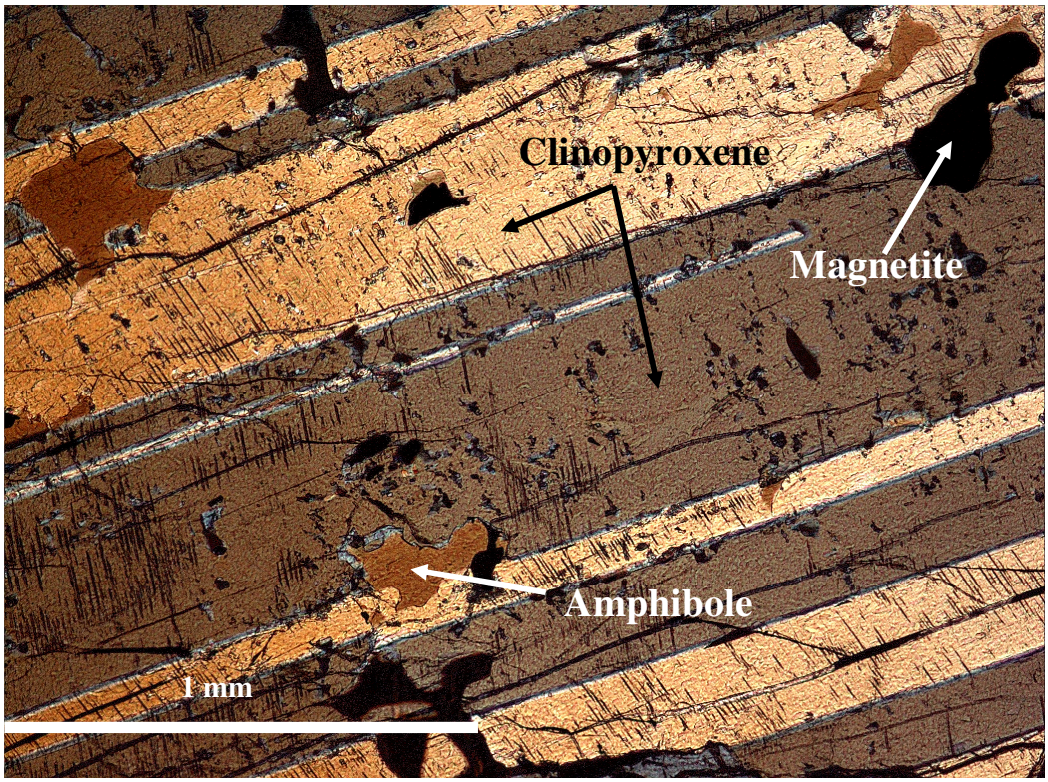

Figure 5.1: Twinned clinopyroxene in IRUP displaying "patchy" alteration to amphibole. Grains of magnetite frequently accompany this type of alteration (thin section MAR 5N). Crossed polars.

Olivine is generally euhedral and fresh, while small amounts of serpentinization are present close to grain edges or along irregularly oriented cracks. In some thin sections, olivine contains linear arrangements of magnetite. Further investigation revealed that the magnetite appears to be intergrown (similar to symplectic intergrowth) with orthopyroxene (Figures 5.2 and 5.3). Occurrences of such intergrowths in olivine are further discussed in Chapter 8.

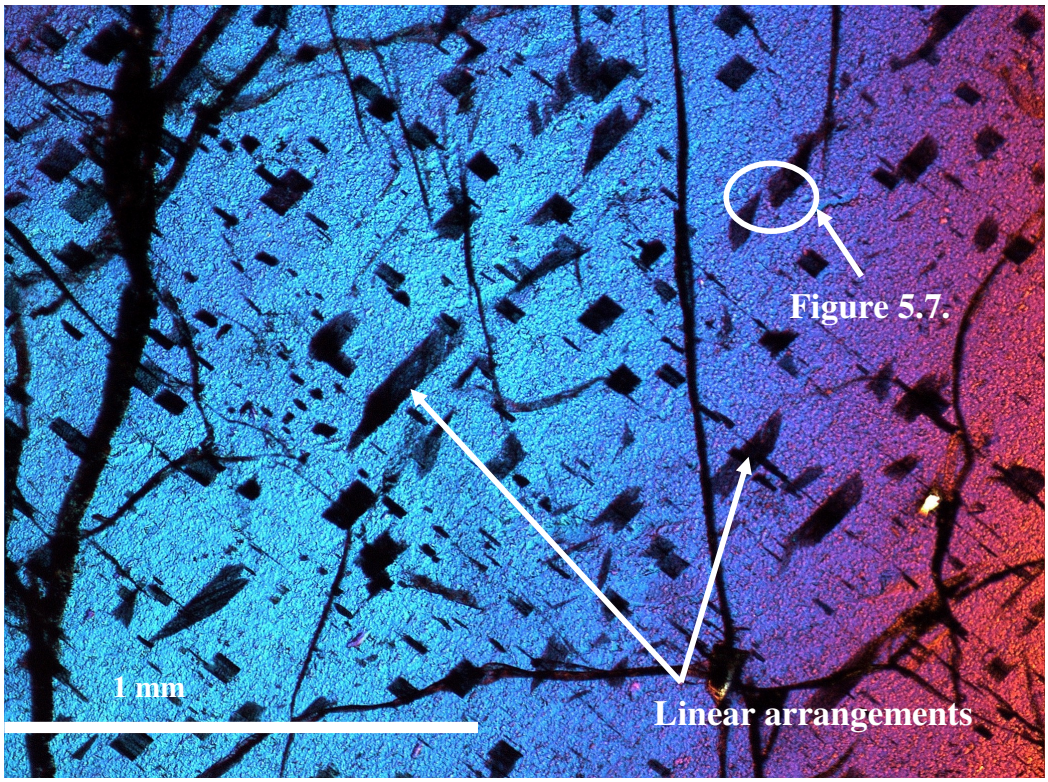

Figure 5.2: Linear arrangements of symplectic intergrowth between magnetite and orthopyroxene in olivine (thin section SAR 1K). Crossed polars.

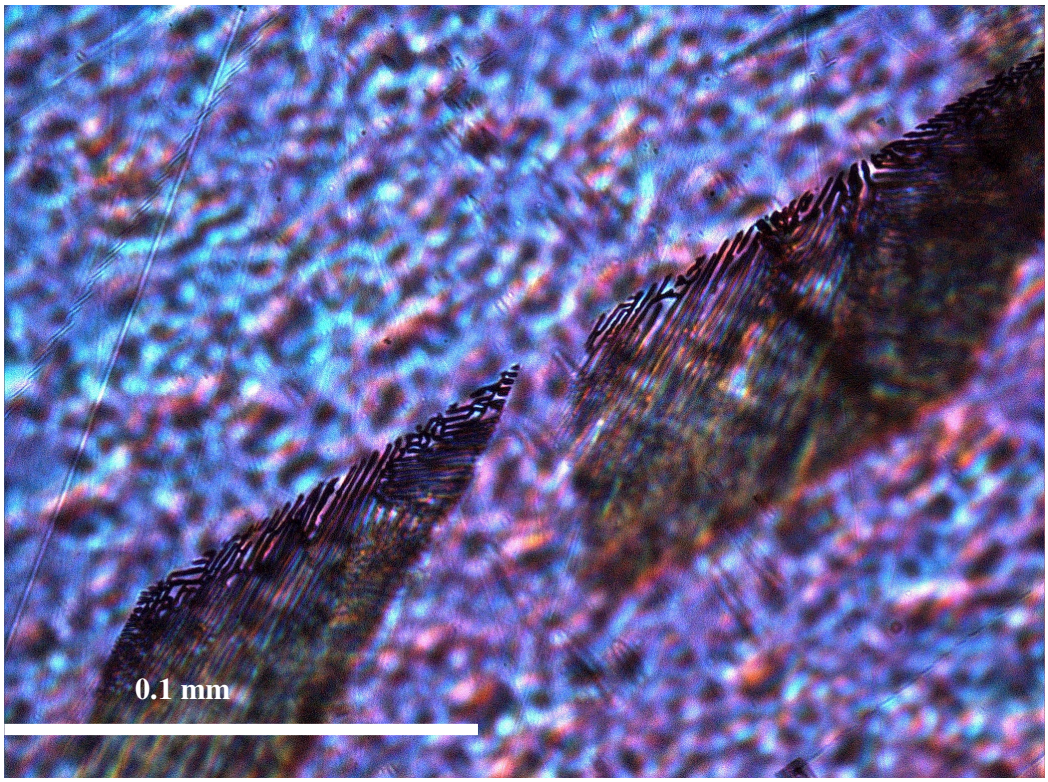

Figure 5.3: Symplectic intergrowths of magnetite and orthopyroxene in olivine (thin section SAR 1K). Crossed polars.

Plagioclase is mostly subhedral and recrystallized exhibiting multiple, and often disturbed, directions of twinning (Figure 5.4). Plagioclase may occur as large grains (Figure 5.5) or as small, irregularly shaped grains. Large plagioclase grains form patches on cm-scale and often poikilitically enclose small rounded grains of pyroxene (Figure 6).

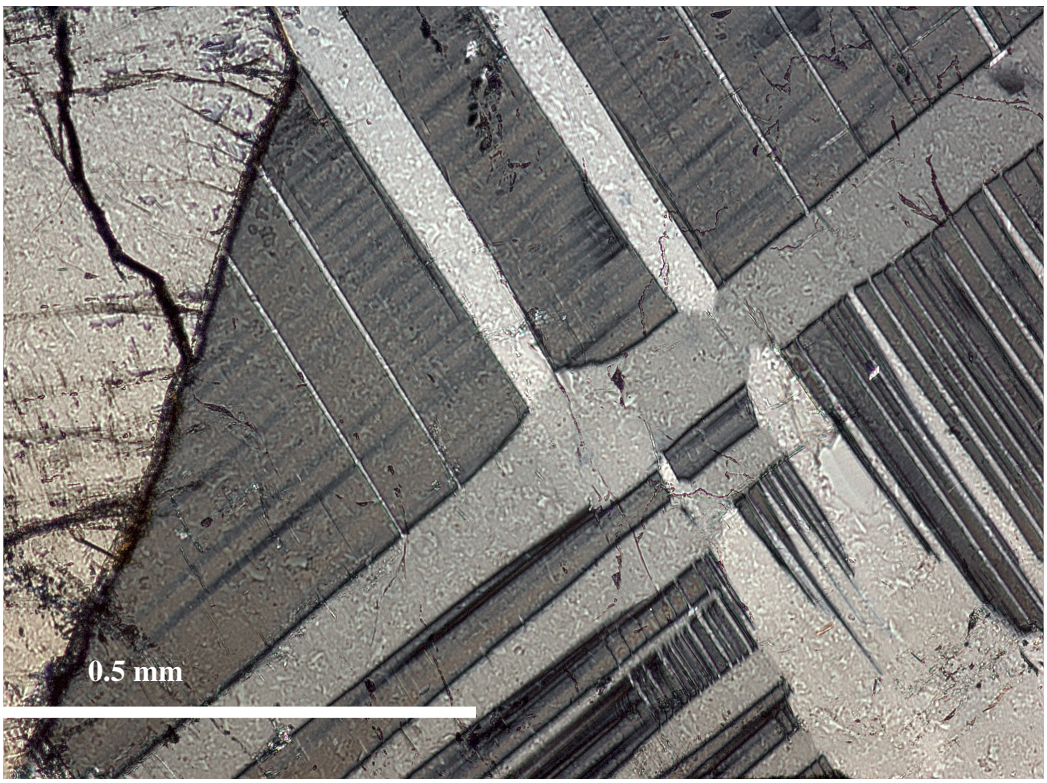

Figure 5.4: Recrystallized plagioclase with disturbed twinning orientations (thin section SAR 1K). Crossed polars.

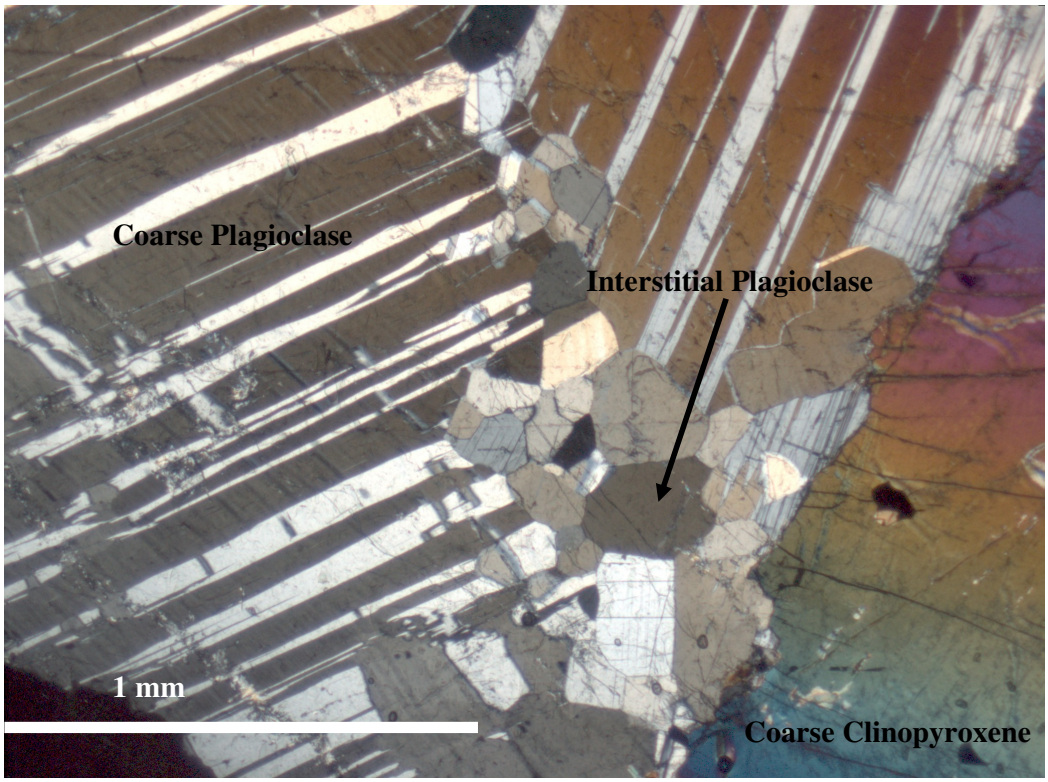

Figure 5.5: Smaller grains of plagioclase interstitial to coarse grains of plagioclase and clinopyroxene (thin section 7B). Crossed polars.

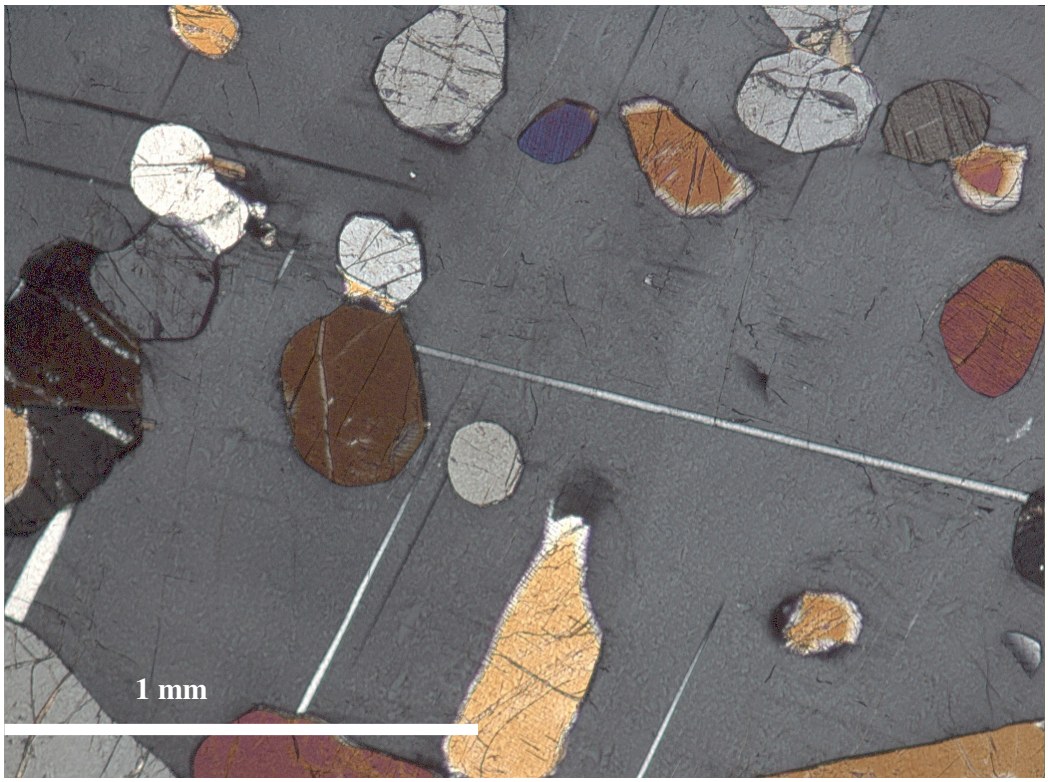

Figure 6: A large plagioclase grain poikilitically enclosing smaller rounded grains of pyroxene (thin section MAR 3Q). Crossed polars.

Analytical Techniques and Sample Preparation

X-Ray Fluorescence (XRF):

Samples were analysed for whole rock composition at the University of Pretoria. XRF sample preparation followed standard procedure: samples were ground to <0.075mm in a carbon steel milling vessel; dried at 100°C for a period of 24 hours, and roasted at 1000°C for 24 hours to determine Loss On Ignition (LOI). After adding 1g sample-powder to 6g $Li_2B_4O_7$ flux, the mixtures were fused into glass beads at 1050°C. Major element analyses were conducted using an ARL9400XP+ spectrometer. Trace element analyses were carried out on pressed powder pellets. XRF analytical results are presented in Appendix C.

X-Ray Diffraction (XRD):

Selected IRUP samples were analysed by XRD, Rietveld analysis, for confirmation of their mineral assemblages, at the University of Pretoria. Instrument and data collection parameters were as follows:

Instrument	:	Siemens D-501
Radiation	:	Cu *Kα* (λ=1.5418 Å)
Temperature	:	25 °C
Specimen	:	flat-plate, rotating (30 RPM)
Power Setting	:	40 kV, 40 mA

Electron Microprobe Analyses (EMPA):

Polished thin sections were used to study the chemical composition of mainly plagioclase, pyroxene (dominantly clinopyroxene), selected amphibole* and olivine in both host cumulate rock and IRUP samples. Analyses were performed using the CAMECA SX100 at the University of Pretoria. An approximately 25 nm thick carbon coating (peacock colour on a brass block) was applied to the polished sections.

Operating conditions were as follows:

Accelerating Potential	:	20kV
Beam Current	:	$2 \cdot 10^{-8}$ A
Counting Time	:	20 seconds
Beam Diameter	:	≈ 0.5 µm
Standards	:	Albite for Na
		Orthoclase for K
		Wollastonite for Si and Ca
		Almandine for Al and Fe
		Periclase for Mg
		NiO for Ni
		Rhodonite for Mn
		Cr_2O_3 for Cr
		Rutile for Ti
Corrections	:	Model XPHI CAMECA Correction Program

* Amphibole is not a major constituent of the host rocks or IRUP. The amphiboles exist as patches of alteration in pyroxene in the IRUP.

Analytical Results

Mineral Assemblage Analyses:

Due to the variability of IRUP mineralogy, XRD analyses were performed on selected IRUP samples to confirm the mineral assemblages identified during petrographic investigations. The results of the XRD analyses are displayed in Table 1.

Table 1: XRD results of selected IRUP samples in wt %

	Sample 24 (IRUP)	Sample 26 (IRUP)	Sample 40 (IRUP)	Sample 49 (IRUP)	Sample 50 (IRUP)
Clinopyroxene	62.3 % +/- 3 %	61.7 % +/- 4.5 %	60.7 % +/- 3.60 %	25.3 % +/- 3.3 %	18.77 % +/- 3 %
Orthopyroxene	3.63 % +/- 2.34 %	6.8 % +/- 4.5 %	7.6 % +/- 3.3 %	4.4 % +/- 4.5 %	4.1 % +/- 3.3 %
Olivine	5.41 % +/- 1.08 %	2.44 % +/- 1.08 %	6.27 % +/- 1.11 %	3.46 % +/- 1.68 %	13.65 % +/- 1.74 %
Plagioclase	20.84 % +/- 2.70 %	21.8 +/- 3.3 %	14.2 % +/- 3.3 %	58.1 % +/- 4.2 %	54.4 % +/- 3.9 %
Magnetite	0.35 % +/- 0.78 %	0.89 % +/- 0.81 %	2.03 % +/- 0.99 %	1.23 % +/- 0.87 %	2.01 % +/- 0.93 %
Actinolite	7.44 % +/- 1.59 %	6.27 % +/- 2.58 %	7.06 % +/- 2.01%	6.49 % +/- 2.25 %	6.18 % +/- 2.16 %
Biotite	.	.	1.65 % +/- 1.14 %	0.98 % +/- 1.47 %	0.65 % +/- 1.47 %

The results indicate that IRUP consists predominantly of clinopyroxene, olivine, plagioclase, magnetite, actinolite, and biotite. The implied reliability of results should be taken into consideration. The error for biotite, a mineral not identified during petrographic investigations, is in most cases larger than the actual amount of biotite detected. It should also be noted that amphibole was identified as an alteration product of pyroxene and that no other discrete amphibole grains were observed during petrographic investigations.

The Whole Rock Chemistry of Samples with Host Rock in Gradual Contact with IRUP:

Sample Set "MAR" (Mottled Anorthosite in Gradual Contact with IRUP):

In this length of drill core (represented by sample numbers 1 to 18), mottled anorthosite appears to be progressively replaced by IRUP. Figure 7.1 indicates that there are several changes with respect to major element oxides when mottled anorthosite is replaced by IRUP. Changes include a decrease in the weight % of

Al_2O_3, which is accompanied by decreases in the weight % of Na_2O and SiO_2. The weight % of Fe_2O_3, MgO, and TiO_2 increases, while the weight % of CaO remains fairly constant along the profile.

There are not only differences between the whole rock chemistry of mottled anorthosite and IRUP, but also within the IRUP itself. At 230.26 m (the midpoint of sample number 9), the whole rock chemistry is similar to that of sample numbers 16 to 18 (229.08 m to 228.8 m). In between these samples, from sample number 10 (at 230.05 m) to sample number 15 (at 229.28 m), further changes occur in a section of the profile that shows more pronounced decreases in the weight % Al_2O_3, Na_2O, and SiO_2, and a more pronounced increase in the weight % of Fe_2O_3, MgO, and TiO_2.

Figure 7.2 illustrates the changes in the trace element values during the replacement of mottled anorthosite by IRUP. The trace element profile indicates both increases and decreases in the concentration of certain trace elements. Cr, Ni, V, and Zr all show increases, while the Sr value decreases along the length of the borehole.

Although it is not as clear as in the element oxide profile, the trace element profile also indicates that there are certain IRUP samples with more pronounced changes in its chemistry. The Cr and V values are quite variable and not suited to reliably indicate the section of more dramatic change. The Ni and Sr values, however, clearly indicate that the trace element chemistry of sample number 9 (at 230.26 m) is similar to that of sample numbers 16 to 18 (at 229.08 m to 228.8 m). In between these samples, from sample number 10 (at 230.05 m) to sample number 15 (at 229.28 m), further changes occur in a section of the profile that shows a more pronounced increase in the ppm values of Ni, and a more pronounced decrease in the ppm values of Sr.

Figure 7.3a, b, and c are profiles illustrating the changes in the normative mineralogy as IRUP replaces mottled anorthosite. The plagioclase profile (Figure 7.3a) indicates that the volume % of the albite component decreases significantly, while the volume % of the anorthite component remains approximately constant along the length of drill core. Figure 7.3b, the olivine profile, shows that the forsterite and fayalite volume % are very similar and that they change in approximately the same proportion. Figure 7.3c is the pyroxene profile, which indicates that there is an increase in the volume % of all three end-members as IRUP replaces mottled anorthosite. The most abundant end-member is wollastonite, followed by enstatite and ferrosilite of which the values are very similar. These data imply that there is an increase in the modal proportion of clinopyroxene, which compliments the results of the petrographic investigations.

Sample Set "SAR" (Spotted Anorthosite in Gradual Contact with IRUP):

This length of drill core is represented by sample numbers 19 to 26, where spotted anorthosite appears to be progressively replaced by IRUP. Figure 7.4 is a profile of the whole rock chemistry along the length of drill core. It shows that as spotted anorthosite is replaced by IRUP, there is a decrease in the weight percentage of Al_2O_3, Na_2O, and SiO_2. Increases include the weight percentages of Fe_2O_3, TiO_2, and CaO. Interestingly, the MgO weight percentage shows only very slight changes and appears to remain generally constant along the length of drill core.

Figure 7.5 is a profile of the trace element values along the length of the drill core. It indicates that there is a decrease in the ppm values of Cr and Sr. While the Zr and V values increase, the Ni content appears to remain approximately constant as the spotted anorthosite is replaced by IRUP.

Figure 7.6a, b and c are profiles indicating the normative mineralogy changes as IRUP replaces the spotted anorthosite host rock. Figure 7.6a, the plagioclase profile, shows that as IRUP replaces the spotted anorthosite the volume % value of the anorthite component decreases, whereas the albite component increases briefly before decreasing. The olivine profile (Figure 7.6b) indicates that the first sample of spotted anorthosite and the last two samples of IRUP have fairly similar volume % values for both the forsterite and fayalite end-members. The remaining samples indicate that there is an increase in volume % values of both end-members from spotted anorthosite to IRUP, with forsterite being more abundant than fayalite in the IRUP itself. Figure 7.6c is the profile of pyroxene, which shows that the replacement of spotted anorthosite by IRUP is accompanied by an increase in all three end-members (wollastonite, enstatite and ferrosilite). Within IRUP itself, wollastonite is most abundant followed by enstatite and ferrosilite. These data imply that there is an increase in the modal proportion of clinopyroxene, which compliments the results of the petrographic investigations.

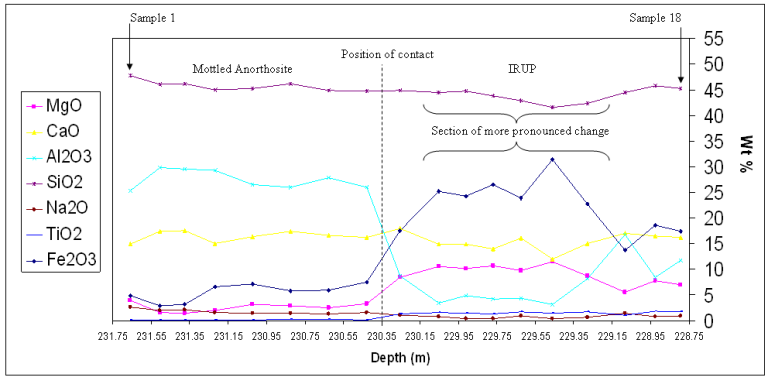

Figure 7.1: Major element oxide profile (from sample numbers 1 to 18) of the length of drill core ("MAR") in which mottled anorthosite is replaced by IRUP. The standard deviation and three sigma values (in wt%, as reported by the X-ray Analytical Laboratory, at the University of Pretoria), is provided in the table below.

	Fe_2O_3	MgO	CaO	Al_2O_3	SiO_2	Na_2O	TiO_2
std dev.(wt %)	0.3	0.1	0.07	0.3	0.4	0.11	0.03
3σ	0.9	0.3	0.21	0.9	1.2	0.33	0.09

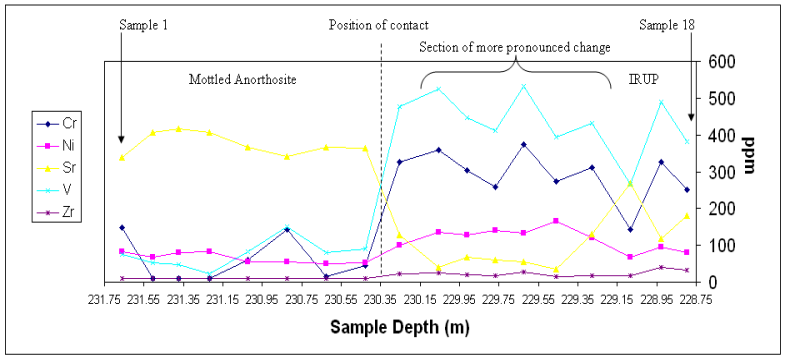

Figure 7.2: Trace element profile (from sample numbers 1 to 18) of the length of drill core ("MAR") in which mottled anorthosite is replaced by IRUP. The three sigma values (in ppm, as reported by the X-ray Analytical Laboratory, at the University of Pretoria), is provided in the table below.

	Cr	Ni	Sr	V	Zr
3σ	120	18	12	30	18

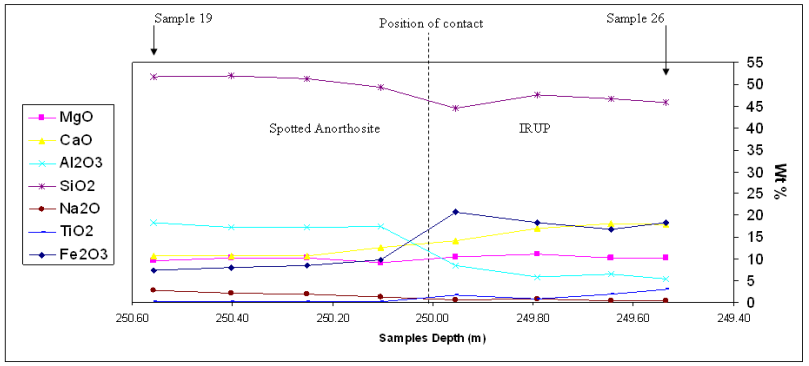

Figure 7.4: Major element oxide profile (from sample numbers 19 to 26) of the length of drill core ("SAR") in which spotted anorthosite is replaced by IRUP. The standard deviation and three sigma values (in wt%, as reported by the X-ray Analytical Laboratory, at the University of Pretoria), is provided in the table below.

	Fe_2O_3	MgO	CaO	Al_2O_3	SiO_2	Na_2O	TiO_2
std dev.(wt%)	0.3	0.1	0.07	0.3	0.4	0.11	0.03
3σ	0.9	0.3	0.21	0.9	1.2	0.33	0.09

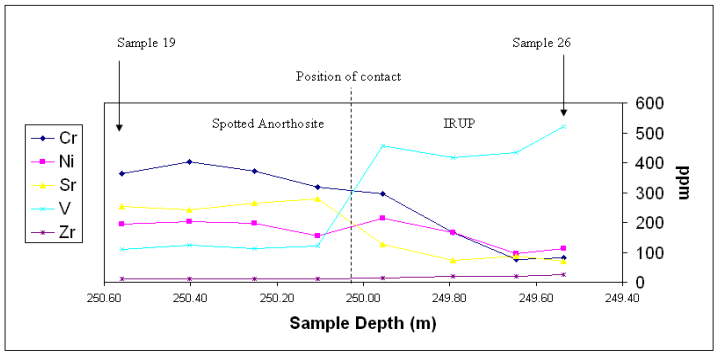

Figure 7.5: Trace element profile (from sample numbers 19 to 26) of the length of drill core ("SAR") in which spotted anorthosite is replaced by IRUP. The three sigma values (in ppm, as reported by the X-ray Analytical Laboratory, at the University of Pretoria), is provided in the table below.

	Cr	Ni	Sr	V	Zr
3σ	120	18	12	30	18

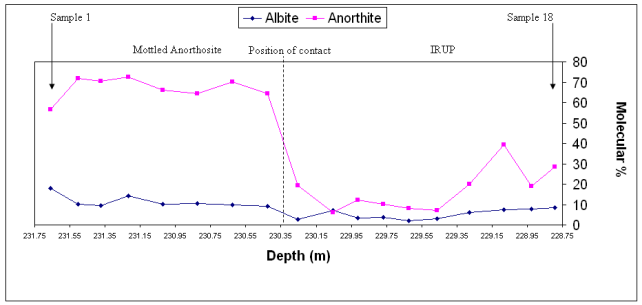

Figure 7.3a: Normative plagioclase profile (from sample numbers 1 to 18) of the length of drill core ("MAR") in which mottled anorthosite is replaced by IRUP.

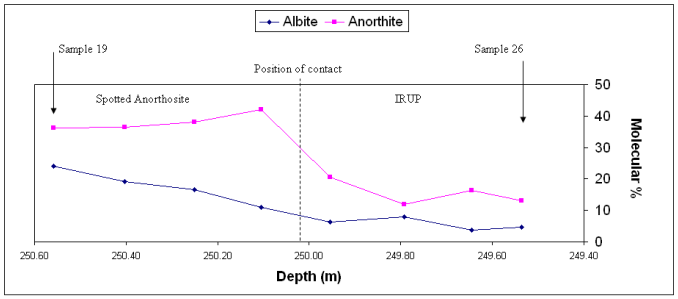

Figure 7.6a: Normative plagioclase profile (from sample numbers 19 to 26) of the length of drill core ("SAR") in which spotted anorthosite is replaced by IRUP.

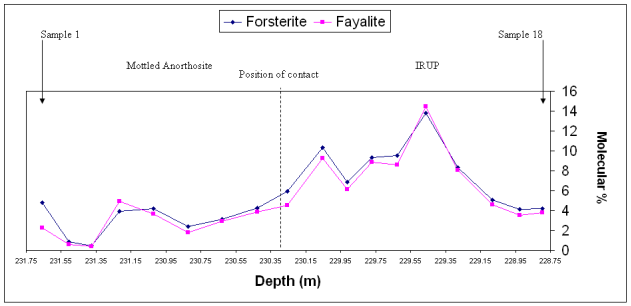

Figure 7.3b: Normative olivine profile (from sample numbers 1 to 18) of the length of drill core ("MAR") in which mottled anorthosite is replaced by IRUP.

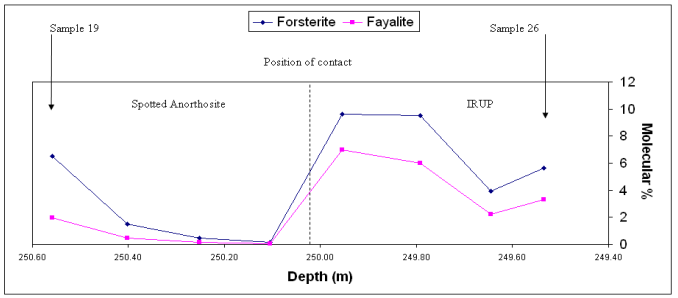

Figure 7.6b: Normative olivine profile (from sample numbers 19 to 26) of the length of drill core ("SAR") in which spotted anorthosite is replaced by IRUP.

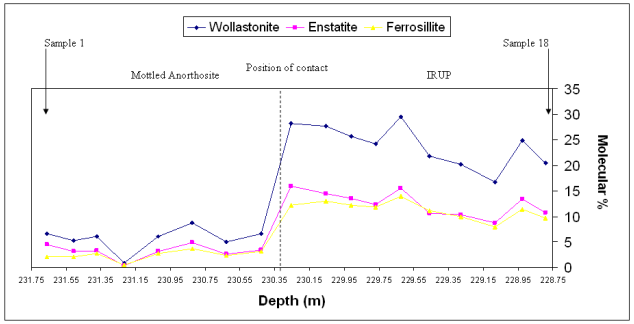

Figure 7.3c: Normative pyroxene profile (from sample numbers 1 to 18) of the length of drill core ("MAR") in which mottled anorthosite is replaced by IRUP.

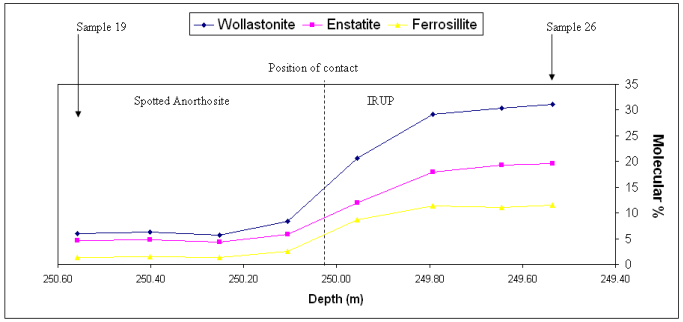

Figure 7.6c: Normative pyroxene profile (from sample numbers 19 to 26) of the length of drill core ("SAR") in which spotted anorthosite is replaced by IRUP.

The Whole Rock Geochemistry of Samples with Host Rock in Sharp Contact with IRUP:

In addition to samples with gradual contacts between IRUP and the host rock, there are also samples with sharp contacts between IRUP and host rock. Sample number 43 represents mottled anorthosite in sharp contact with the IRUP of sample number 44. Sample number 45 represents spotted anorthosite in sharp contact with the IRUP of sample number 46.

Figures 7.9a and b are X-Y charts showing the main differences in major element oxide chemistry between the host rock and IRUP. A comparison between mottled anorthosite (sample number 43) and IRUP (sample number 44) in Figure 7.9a, reveals that the mottled anorthosite has higher SiO_2, Al_2O_3, CaO, and Na_2O wt % values than the IRUP, while the IRUP body is enriched in Fe2O3 and MgO. A comparison between spotted anorthosite (sample number 45) and IRUP (sample number 46) in Figure 7.9b, reveals similar chemical changes. The spotted anorthosite is richer in Al_2O_3, Na_2O, and SiO_2, although the difference between the SiO_2 content of spotted anorthosite and IRUP is only 2.1 wt %. The IRUP, however, is richer in Fe_2O_3, MgO, and CaO.

The trace element geochemistry of the samples associated by sharp contacts is illustrated in Figures 7.10a and b. From these diagrams it is evident that there are not only chemical differences between the host rock and the IRUP, but also between the spotted and mottled anorthosite. The spotted anorthosite is richer in Cr and Ni, while it contains slightly less Sr than the mottled anorthosite. Both IRUPs in contact with mottled and spotted anorthosite respectively are richer in Cr, Ni and V, wile the Sr values are lower than that of the host rock. Differences in Zr values remain within 3σ (18ppm) of the analytical reproducibility. Zr values are therefore effectively constant.

Figures 7.11a and b show the normative mineralogy for spotted and mottled anorthosite and their associated IRUP. IRUP is enriched in all pyroxene and olivine end-members and shows low values for both albite and anorthite compared to their host rocks.

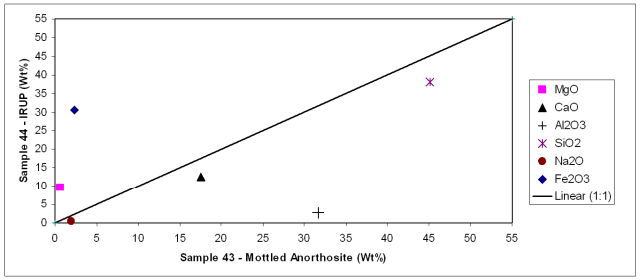

Figure 7.9a: The major element oxide chemistry of host rock and IRUP associated by a sharp contact. Sample number 43 is mottled anorthosite in sharp contact with the IRUP of sample number 44 (contact at 446.43m drilling depth). The standard deviation and three sigma values (in wt%, as reported by the X-ray Analytical Laboratory, at the University of Pretoria), is provided in the table below.

	Fe_2O_3	MgO	CaO	Al_2O_3	SiO_2	Na_2O	TiO_2
std dev.(wt%)	0.3	0.1	0.07	0.3	0.4	0.11	0.03
3σ	0.9	0.3	0.21	0.9	1.2	0.33	0.09

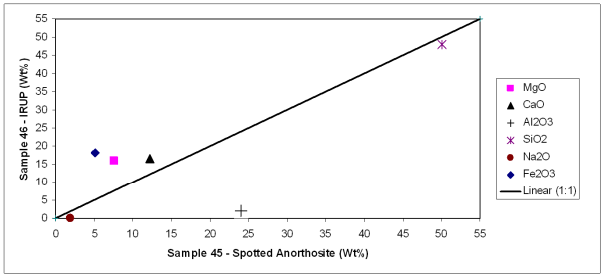

Figure 7.9b: The major element oxide chemistry of host rock and IRUP associated by a sharp contact. Sample number 45 is spotted anorthosite in sharp contact with the IRUP of sample number 46 (contact at 665.05m drilling depth). The standard deviation and three sigma values (in wt%, as reported by the X-ray Analytical Laboratory, at the University of Pretoria), is provided in the table below.

	Fe_2O_3	MgO	CaO	Al_2O_3	SiO_2	Na_2O	TiO_2
std dev.(wt%)	0.3	0.1	0.07	0.3	0.4	0.11	0.03
3σ	0.9	0.3	0.21	0.9	1.2	0.33	0.09

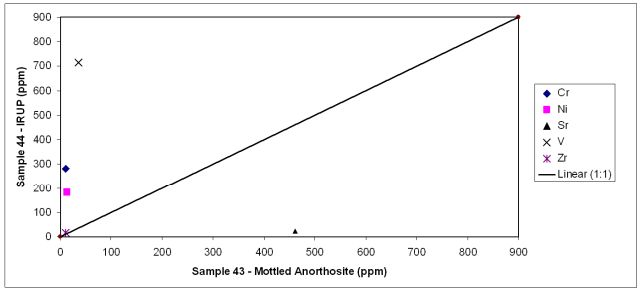

Figure 7.10a: Indicating the differences in trace element geochemistry between host rock and IRUP associated by a sharp contact. Sample number 43 is mottled anorthosite in sharp contact with the IRUP of sample number 44 (contact at 446.43m drilling depth). The three sigma values (in ppm, as reported by the X-ray Analytical Laboratory, at the University of Pretoria), is provided in the table below.

	Cr	Ni	Sr	V	Zr
3σ	120	18	12	30	18

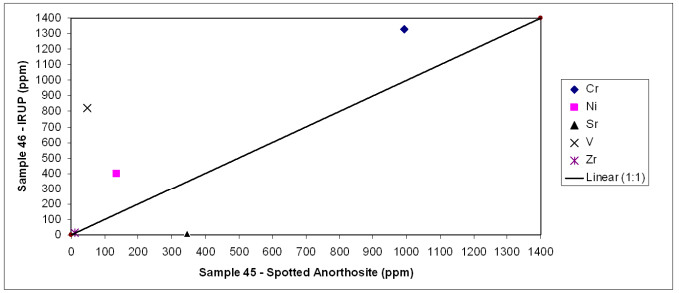

Figure 7.10b: Indicating the differences in trace element geochemistry between host rock and IRUP associated by a sharp contact. Sample number 45 is spotted anorthosite in sharp contact with the IRUP of sample number 46 (contact at 665.05m drilling depth). The three sigma values (in ppm, as reported by the X-ray Analytical Laboratory, at the University of Pretoria), is provided in the table below.

	Cr	Ni	Sr	V	Zr
3σ	120	18	12	30	18

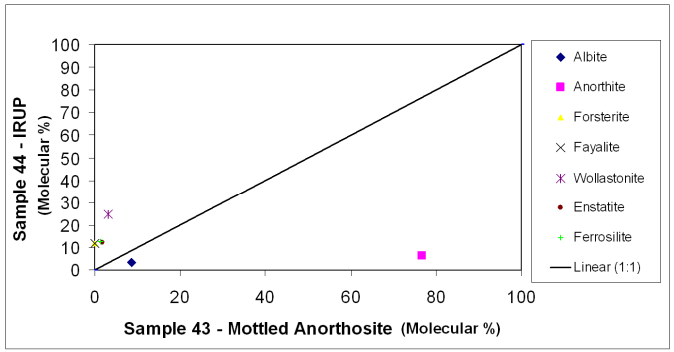

Figure 7.11a: Normative mineralogy of sample number 43 (mottled anorthosite) in sharp contact with sample number 44 (IRUP). Contact at 446.43m drilling depth.

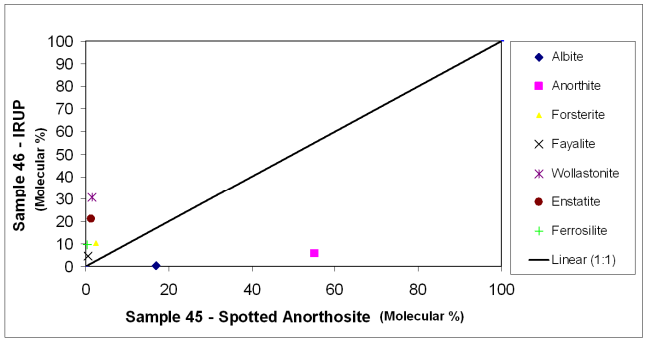

Figure 7.11b: Normative mineralogy of sample number 45 (spotted anorthosite) in sharp contact with sample number 46 (IRUP). Contact at 665.05m drilling depth.

Comparison between the Whole Rock Chemistry of Unreplaced Host Rock and IRUP:

Samples from equal stratigraphic levels, from two different boreholes, were used to compare the geochemistry of unreplaced host rocks and IRUP. Figure 7.12 illustrates the major element oxide chemistry of these samples. The IRUP samples have lower SiO_2, Al_2O_3, and Na_2O wt % values compared to the unreplaced host rocks. All IRUP samples show increased Fe_2O_3, CaO, and MgO (except IRUP sample number 40, which has a slightly lower MgO content) compared to the unreplaced host rocks.

The trace element chemistry of these samples are illustrated in Figure 7.13, which shows that IRUP samples have lower ppm values for Cr, Sr, and Ni (except IRUP sample number 40), while the IRUP samples are richer in V, with an effectively constant Zr content compared to the unreplaced host rocks.

The changes in whole rock chemistry are also reflected in the normative mineralogy (Figure 7.14). All IRUP samples have higher values in forsterite, fayalite, wollastonite, enstatite and ferrosilite, while the volume % values for albite and anorthite are lower compared to the unreplaced mottled and spotted anorthosite.

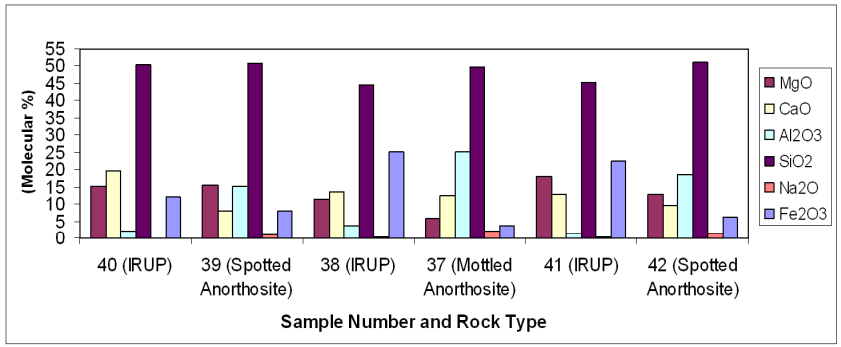

Figure 7.12: The major element oxide chemistry of unreplaced host rock and IRUP samples at equal stratigraphic levels. The standard deviation and three sigma values (in wt%, as reported by the X-ray Analytical Laboratory, at the University of Pretoria), is provided in the table below.

	Fe_2O_3	MgO	CaO	Al_2O_3	SiO_2	Na_2O	TiO_2
std dev.(wt%)	0.3	0.1	0.07	0.3	0.4	0.11	0.03
3σ	0.9	0.3	0.21	0.9	1.2	0.33	0.09

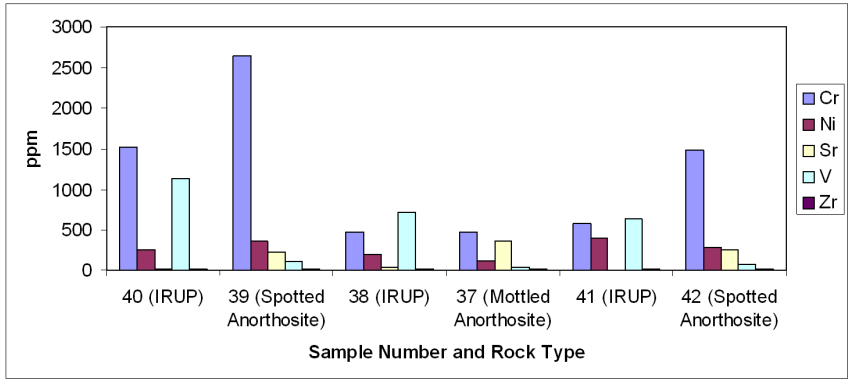

Figure 7.13: The trace element chemistry of unreplaced host rock and IRUP samples at equal stratigraphic levels. The three sigma values (in ppm, as reported by the X-ray Analytical Laboratory, at the University of Pretoria), is provided in the table below.

	Cr	Ni	Sr	V	Zr
3σ	120	18	12	30	18

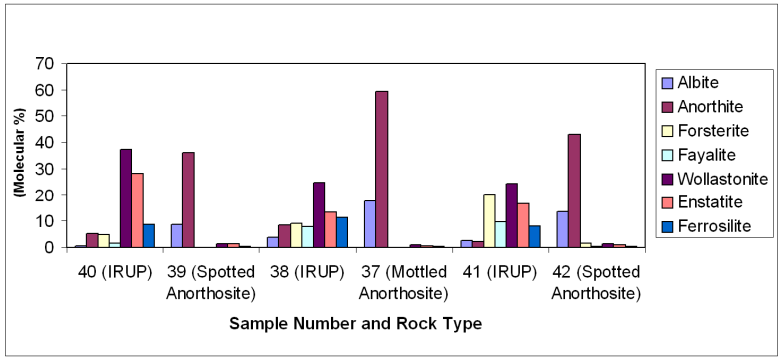

Figure 7.14: The normative mineralogy of unreplaced host rocks and IRUP samples at equal stratigraphic levels.

The Whole Rock Geochemistry of Samples Above and Below the UG2 Chromitite Layer:

The whole rock chemical variation between IRUP samples above and below the UG2 is illustrated in Figure 7.15. The graph illustrates that the IRUP samples closest to the UG2 (above and below) appear to have a different whole rock composition compared to those IRUP sample farthest from the UG2. Two IRUP samples (sample numbers 48 and 49) above the UG2 have quite similar whole rock compositions, while the sample closest to the UG2 (sample number 47) has higher wt % values for Al_2O3, Na_2O, FeO, and Fe_2O_3 and lower values for CaO, MgO, and SiO_2. One of the samples below the UG2 (sample number 50) has a whole rock composition comparable to those of sample numbers 48 and 49 above the UG2, while sample numbers 51 and 52 (closer to the UG2) are comparable to sample number 47.

The trace element chemistry of IRUP samples above and below the UG2 is illustrated in Figure 7.16. Zr values are effectively constant for samples above and below the UG2. Cr and V contents decrease closer to the UG2. Only sample number 47 (closest to and above the UG2) has anomalously lower and higher values for Ni and Sr respectively compared to the other IRUP samples.

Figure 7.17a, b, and c illustrate the normative mineralogy of IRUP samples above and below the UG2. The plagioclase diagram (Figure 7.17a) indicates that sample number 47 (closest to and above the UG2) has increased volume % values for both the anorthite and albite end-members. The olivine normative mineralogy is illustrated in Figure 7.17b. Above the UG2, the volume % of forsterite decreases closer to the UG2, while the fayalite volume % increases. IRUP samples closest to and below the UG2 (samples number 51 and 52) show increased volume % values for both the forsterite and fayalite end-members compared to sample 50 farther below. Figure 7.17c illustrates the normative pyroxene mineralogy. The IRUP sample above and closest to the UG2 has lower volume % values for all three pyroxene end-members, while sample number 51 (the intermediate sample below the UG2) has lower volume % values for wollastonite and enstatite, and a ferrosilite content comparable to the deepest IRUP sample.

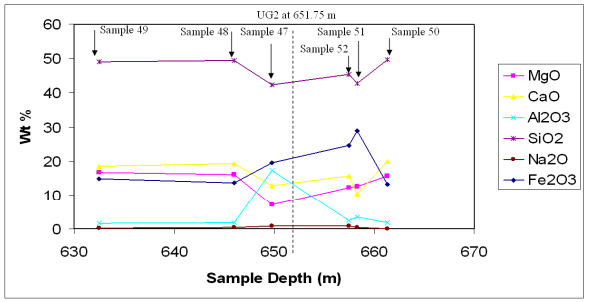

Figure 7.15: The major element oxide chemistry of IRUP samples above and below the UG2 chromitite layer. The standard deviation and three sigma values (in wt%, as reported by the X-ray Analytical Laboratory, at the University of Pretoria), is provided in the table below.

	Fe_2O_3	MgO	CaO	Al_2O_3	SiO_2	Na_2O	TiO_2
std dev.(wt%)	0.3	0.1	0.07	0.3	0.4	0.11	0.03
3σ	0.9	0.3	0.21	0.9	1.2	0.33	0.09

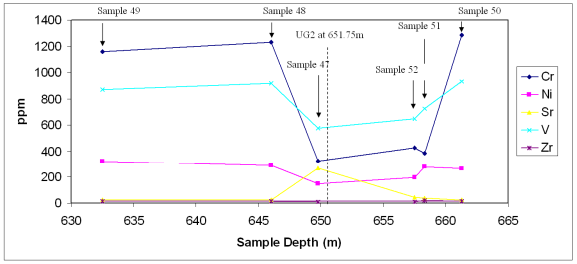

Figure 7.16: The trace element chemistry of IRUP samples above and below the UG2 chromitite layer. The three sigma values (in ppm, as reported by the X-ray Analytical Laboratory, at the University of Pretoria), is provided in the table below.

	Cr	Ni	Sr	V	Zr
3σ	120	18	12	30	18

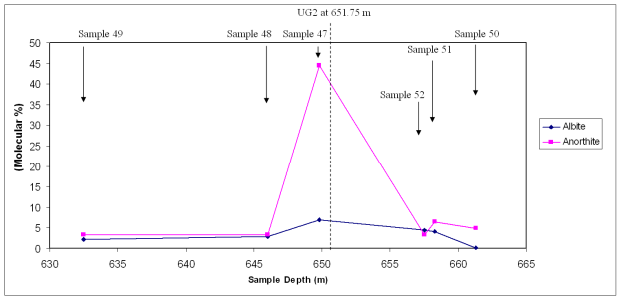

Figure 7.17a: Normative plagioclase mineralogy of IRUP samples above and below the UG2.

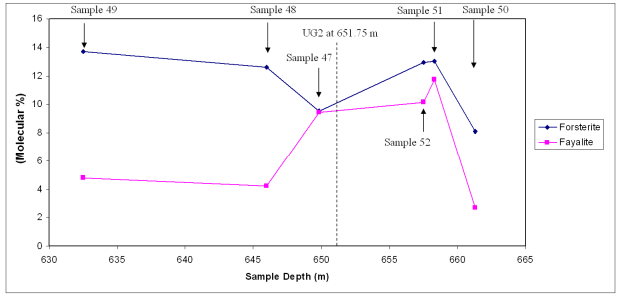

Figure 7.17b: The normative olivine mineralogy of IRUP samples above and below the UG2.

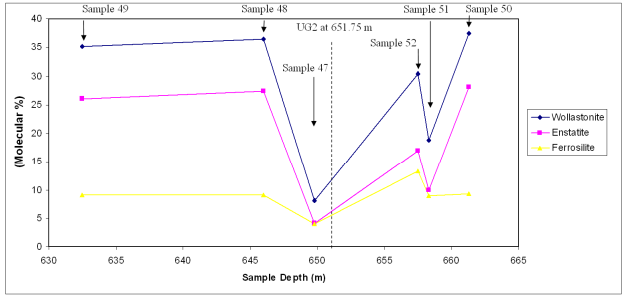

Figure 7.17c: The normative pyroxene mineralogy for IRUP samples above and below the UG2.

The Whole Rock Chemistry of IRUP Samples at Variable Depth:

Figure 7.18 illustrates the variation in major element oxide chemistry in IRUP samples from variable stratigraphic heights. The general trend appears to be that the IRUP samples at shallower stratigraphic levels have slightly lower Fe_2O_3, and MgO contents, with slightly higher CaO, Al_2O_3, Na_2O, and Ti_2O wt % values.

The trace element ppm values for the IRUP samples at variable stratigraphic levels are illustrated in Figure 7.19. The bar chart shows that there is a general decrease in the Cr, Ni, and V contents with an increase in stratigraphic height, while the Sr values increase with height. The differences between Zr values are below the 3σ value.

The normative mineralogy is illustrated in Figure 7.20. The bar chart shows that all three samples at greater depth have lower albite and anorthite volume % values, compared to those samples at shallower depth. The only significant difference in the olivine volume % values between samples at greater and shallower depths is that of sample number 41, which shows an increased forsterite value compared to all other samples. Sample number 23 (at shallower depth) displays the lowest values for all three pyroxene end-members, while sample number 40 (at greatest depth) has the highest values. Generally the samples at greater depth appear to have lower pyroxene values compared to those at shallower depth.

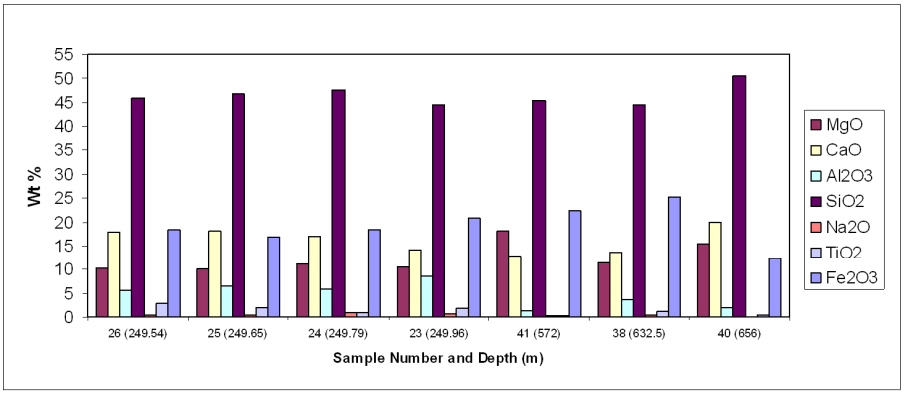

Figure 7.18: The major element oxide chemistry of IRUP samples at variable stratigraphic levels. The standard deviation and three sigma values (in wt%, as reported by the X-ray Analytical Laboratory, at the University of Pretoria), is provided in the table below.

	Fe_2O_3	MgO	CaO	Al_2O_3	SiO_2	Na_2O	TiO_2
std dev.(wt%)	0.3	0.1	0.07	0.3	0.4	0.11	0.03
3σ	0.9	0.3	0.21	0.9	1.2	0.33	0.09

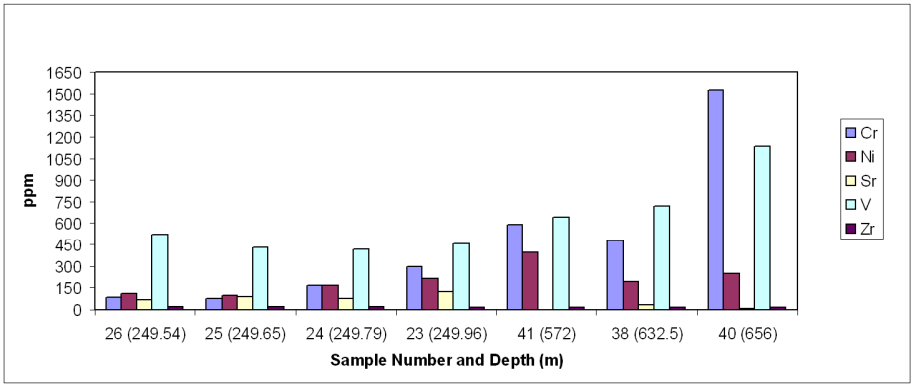

Figure 7.19: The trace element values for IRUP samples at variable stratigraphic levels. The three sigma values (in ppm, as reported by the X-ray Analytical Laboratory, at the University of Pretoria), is provided in the table below.

	Cr	Ni	Sr	V	Zr
3σ	120	18	12	30	18

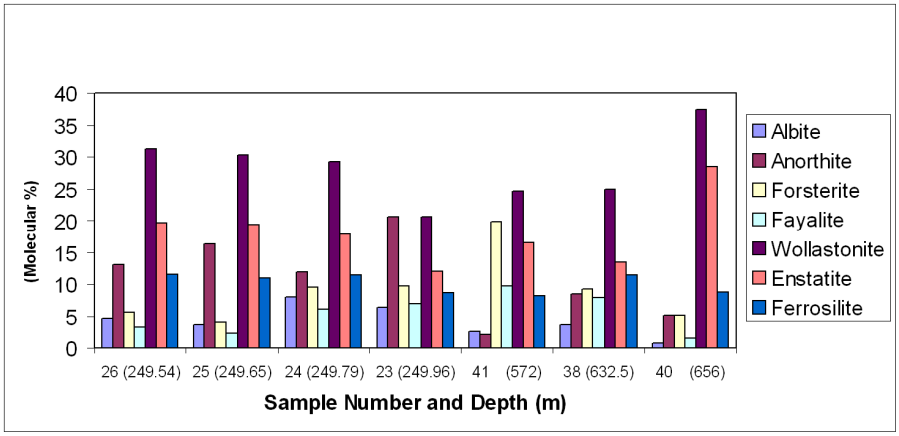

Figure 7.20: The normative mineralogy of IRUP samples at variable depths.

Electron Microprobe Analyses (EMPA):

Electron microprobe analyses were used to determine the composition of feldspar (mainly plagioclase), pyroxene, and olivine in both IRUP and host cumulate rocks.

The following sets of samples were selected for EMPA:

a) Sample set "MAR" from borehole R151,
b) Sample set "SAR" from borehole R14, and
c) Sample numbers 49 and 50 (above and below the UG2 respectively).

In order to simplify the microprobe analytical results each mineral from each of the four sample sets will be considered individually. An average was calculated and plotted for analyses that fall within a 3σ range, for each of the analysed minerals in each thin-section, excluding the results that deviate significantly from the average. In order to clarifying the spread of feldspar and olivine analyses, values for the orthoclase and tephroite end members were multiplied by a factor of 20. Appendix C illustrates the location of thin sections used for EMPA. EMPA data are presented in Appendix D.

Sample "MAR" from borehole R151:

Feldspar:

Figure 7.21 is a ternary diagram with the results of the EMPA of feldspar. Except for a few results, most of the feldspar analyses over the length of the borehole plot in a very small area of the diagram. The analyses that plot away from the average composition contain more of the albite end member, and are from thin sections MAR 7L and MAR 8J, which are the two thin sections located within IRUP material nearest the un-replaced leuconorite.

Olivine:

Figure 7.22 is a ternary diagram illustrating the compositional variation of olivine. In this particular samples set only four thin sections contain olivine, three of which are located within the IRUP material. The fourth thin section is one of mottled anorthosite farthest from the IRUP material i.e. MAR 12B.

Figure 7.22 indicates that there is a significant difference between the olivine composition in the sample located in the leuconorite (MAR 12B) and the olivine composition in the samples from the IRUP material. The difference indicates that

there is a decrease in the atomic proportion of the Mg end member and an increase in the Fe end member as mottled anorthosite is replaced by IRUP. Figure 7.22 also shows that there is no variation in the composition of olivine in the IRUP.

***Pyroxene**:*

Figure 7.23 is a ternary diagram indicating the compositional variation of pyroxene over the length of the borehole. Pyroxene is present in every thin section selected for EMPA. Figure 7.23 illustrates that as the mottled anorthosite is replaced by IRUP, pyroxene becomes richer in the ferrosilite end member. The difference in ferrosilite content, however, is only visible between the thin section farthest from the IRUP material and those closest to and within the IRUP material. Variations in pyroxene composition are clearly visible within individual thin sections. This is due to the high amount of closely spaced exsolution lamellae in the pyroxene grains. It is also noted from Figure 7.23 that the composition of co-existing orthopyroxene and clinopyroxene deviates from the expected compositions as predicted by the orientation of tie lines.

Sample "SAR" from borehole R14:

***Feldspar**:*

Figure 7.24 is a ternary diagram with the results of the EMPA of feldspar. The diagram illustrates that there is a significant difference between the composition of feldspar in the spotted anorthosite and that of the IRUP. Feldspar within the IRUP itself shows very little variation, however, plagioclase from the thin section of IRUP farthest from the unreplaced spotted anorthosite has a slightly lower anorthite content. The thin section of spotted anorthosite farthest from the IRUP shows two distinct compositions, the one richer in the anorthite component than the other.

Olivine

Figure 7.25 is a ternary diagram illustrating the lack of compositional variation of olivine in sample set "SAR", from the host spotted anorthosite to the IRUP.

Pyroxene

The compositional variation of pyroxene in sample set "SAR" is illustrated in Figure 7.26. The results are very similar to that of sample set "MAR". The only significant difference in the composition of pyroxene is between thin section SAR 4A (spotted anorthosite farthest from the IRUP material) and the thin sections either bordering on or within the IRUP material. There is again compositional variation within individual thin sections. These variations are believed to be a result of the closely spaced exsolution lamellae present in the pyroxene.

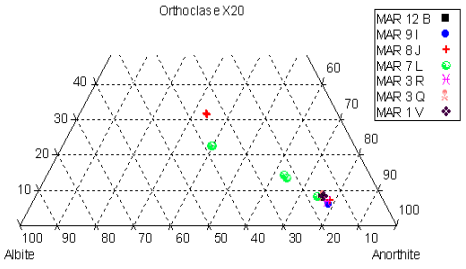

Figure 7.21: The compositional variation of feldspar in sample "MAR" as determined by EMPA. The diagram is plotted with orthoclase X20.

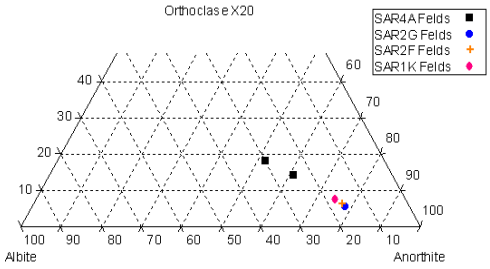

Figure 7.24: The compositional variation of feldspar in sample "SAR" as determined by EMPA. The diagram is plotted with orthoclase X20.

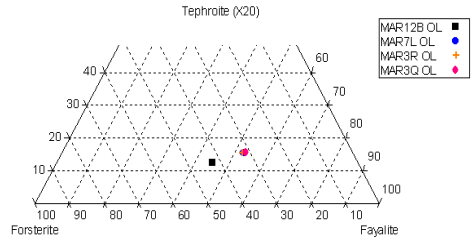

Figure 7.22: The olivine compositional variation in sample "MAR" as determined by EMPA. Note that the tephroite end-member was plotted as tephroite X 20.

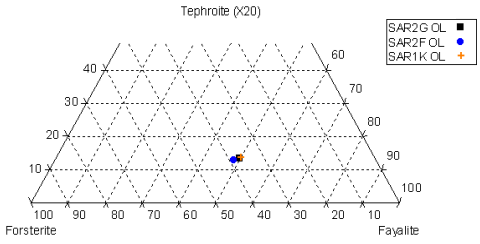

Figure 7.25: The olivine compositional variation in sample "SAR" as determined by EMPA. Note that the tephroite end-member was plotted as tephroite X 20.

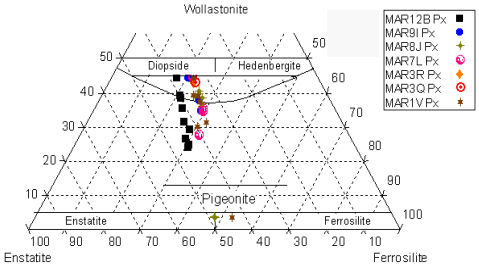

Figure 7.23: The pyroxene compositional variation in sample "MAR" as determined by EMPA (overlay adapted from Klein and Hurlbut, 2000).

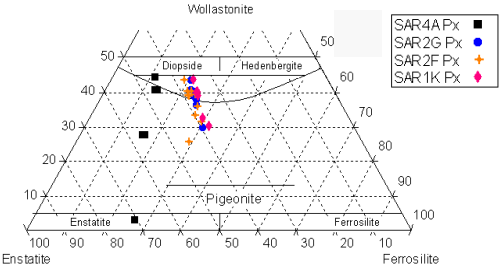

Figure 7.26: The pyroxene compositional variation in sample "SAR" as determined by EMPA (overlay adapted from Klein and Hurlbut, 2000).

Sample numbers 49 and 50 (above and below the UG2 respectively):

Feldspar

The variation in feldspar composition between samples above and below the UG2 is illustrated in Figure 7.28. The diagram shows that there is hardly any variation in the composition of feldspar above and below the UG2. It may however be concluded that feldspar in IRUP below the UG2 (sample number 50) is slightly richer in the anorthite component.

Olivine

Figure 7.29 is a ternary diagram indicating the compositional variation of olivine between samples 49 and 50, above and below the UG2 chromitite layer. Figure 7.29 shows that olivine above the UG2 is more fayalitic compared to those below the UG2.

Pyroxene

The compositional variation of pyroxene between samples number 49 and 50 (above and below the UG2) is illustrated in Figure 7.30. The diagram shows that the pyroxene of sample number 49 (above the UG2) is slightly richer in the ferrosilite component compared to the pyroxene of sample number 50 (below the UG2).

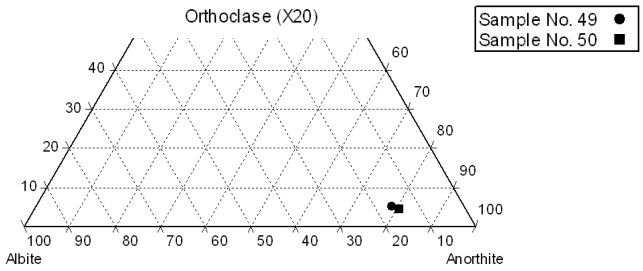

Figure 7.28: The compositional variation of feldspar in samples number 49 and 50 (above and below the UG2) as determined by EMPA. The diagram is plotted with orthoclase X20.

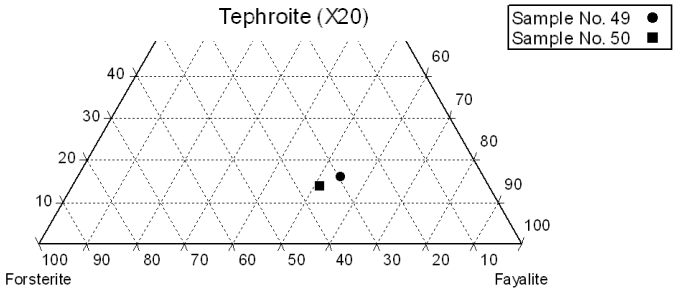

Figure 7.29: The olivine compositional variation in samples number 49 and 50 (above and below the UG2) as determined by EMPA. Note that the tephroite end-member was plotted as tephroite X 20.

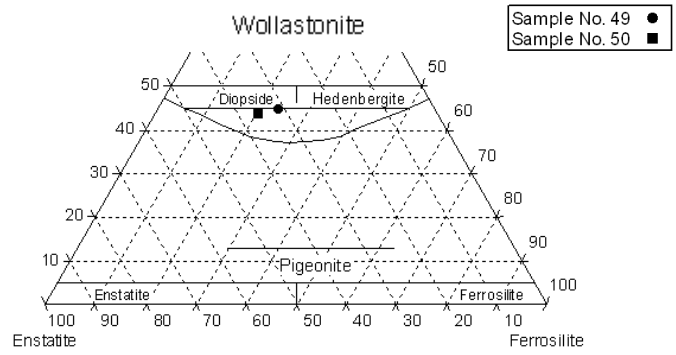

Figure 7.30: The pyroxene compositional variation in samples number 49 and 50 (above and below the UG2) as determined by EMPA (overlay adapted from Klein and Hurlbut, 2000).

Discussion

Whole Rock Chemistry and Element Ratios:

In order to accurately interpret the whole rock chemical changes, as illustrated in Chapter 7, the relative mobility of elements must be taken into account. The fact that the Al_2O_3 wt % values decrease during the formation of IRUP in the host mottled anorthosite does not imply that the total amount of aluminium (number of moles) in the system decreased. Chapter 8.1 investigates the relative mobility of elements, not only to better understand the IRUP formation process, but also to quantify the volume changes associated with IRUP formation.

Figure 8.1a and b illustrates that the Al_2O_3/Sr ratio remains approximately constant throughout sample sets "MAR" and "SAR" respectively. Electron microprobe analyses (discussed in Chapter 8.2) indicated that there is no significant difference between the compositions of plagioclase in mottled anorthosite and the IRUP plagioclase in sample set "MAR", and between the compositions of plagioclase in spotted anorthosite and the IRUP plagioclase of sample set "SAR". The normative mineralogy profiles (Figure 7.3b and 7.3c – sample set "MAR", and Figures 7.6b and 7.6c – sample set "SAR") indicate that there is a significant increase in the amount of olivine and clinopyroxene, while petrographic investigations (Chapter 5) revealed increases of between 5 and 10% in the amount of magnetite from mottled anorthosite and spotted anorthosite to IRUP. Because plagioclase was not affected in composition and volume, it is suggested that aluminium acted as an immobile element and that the decrease in the Al_2O_3 wt % value is a result of a dilution effect caused by the addition of substantial amounts of iron, magnesium, and calcium (accounted for in the increased modal proportions of clinopyroxene). Iron was incorporated into magnetite, olivine, and clinopyroxene, while magnesium found its way into olivine and clinopyroxene, with calcium being mainly included into clinopyroxene. The major element oxide profile of sample set "MAR" (Figure 7.1) does not show an increase in the CaO wt % value from mottled anorthosite to IRUP as it was also affected by dilution caused by the addition of substantial amounts of iron and magnesium, resulting in a relatively constant CaO wt % value.

The major element oxide profile of sample set "SAR" (Figure 7.4) does, however, show an increase in the CaO wt % value from spotted anorthosite to IRUP. This could imply that the fluid responsible for IRUP formation in sample set "SAR" was not as enriched in iron and magnesium, or more enriched in CaO, than the fluid responsible for the formation of IRUP in sample set "MAR".

The Al_2O_3/Fe_2O_3, Al_2O_3/MgO, and Al_2O_3/CaO ratios for sample set "MAR" are illustrated in Figure 8.2a, b, and c, while the Al_2O_3/Fe_2O_3, Al_2O_3/MgO, and Al_2O_3/CaO ratios for sample set "SAR" are illustrated in Figures 8.3a, b, and c. Figures 8.2 and 8.3 show that the Al_2O_3/Fe_2O_3, Al_2O_3/MgO, and Al_2O_3/CaO ratios decrease from mottled anorthosite and spotted anorthosite to IRUP.

Assuming that aluminium was an immobile element during the formation of IRUP, the gains and/or losses for every IRUP sample in sample sets "MAR" and "SAR" were calculated using Gresens' equation (equation 2) for metasomatic alteration (Gresens, 1967). The results of the calculations are illustrated in Figure 8.4a and b.

$$100\left[f_v\left(\frac{gB}{gA}\right)c_n^B - c_n^A\right] = x_n \qquad \text{(equation 2)}$$

Figure 8.4a shows some variation in the gains of the major element oxides in IRUP samples from sample set "MAR". Figure 8.4a indicates that samples 10-14 are enriched in SiO_2, MgO, Fe_2O_3, and CaO, compared to the other IRUP samples from sample set "MAR". The major element oxide profile (Figure 7.1) also indicated an area of more pronounced increases in the wt % values of SiO_2, MgO, Fe_2O_3, and CaO. It is subsequently suggested that the formation of IRUP was probably a multi-stage event where IRUP rocks (formed during, for example, stage one of the alteration process) were further altered by one or more subsequent stages of alteration, thereby resulting in areas or zones of varying degrees of alteration.

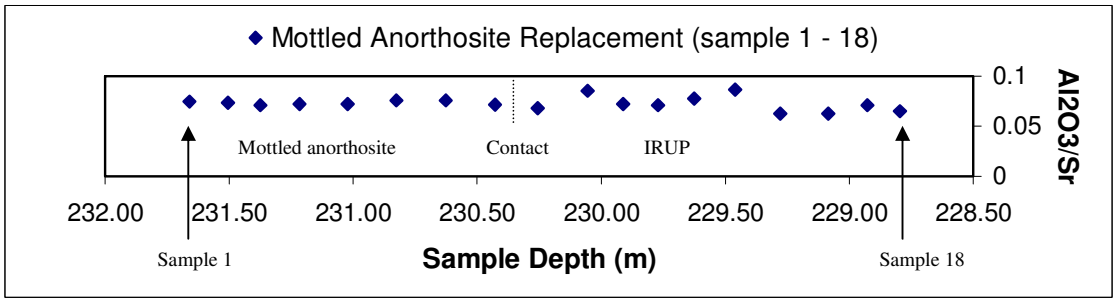

Figure 8.1a: The Al_2O_3/Sr ratio of sample set "MAR" where mottled anorthosite is replaced by IRUP.

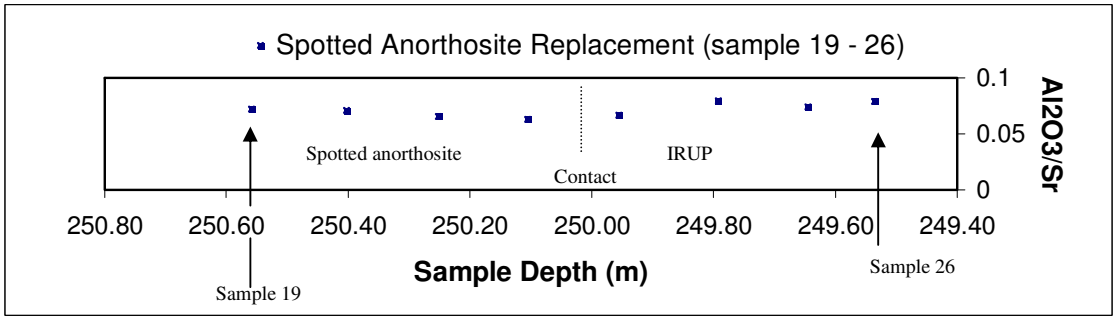

Figure 8.1b: The Al_2O_3/Sr ratio of sample set "SAR" where spotted anorthosite is replaced by IRUP.

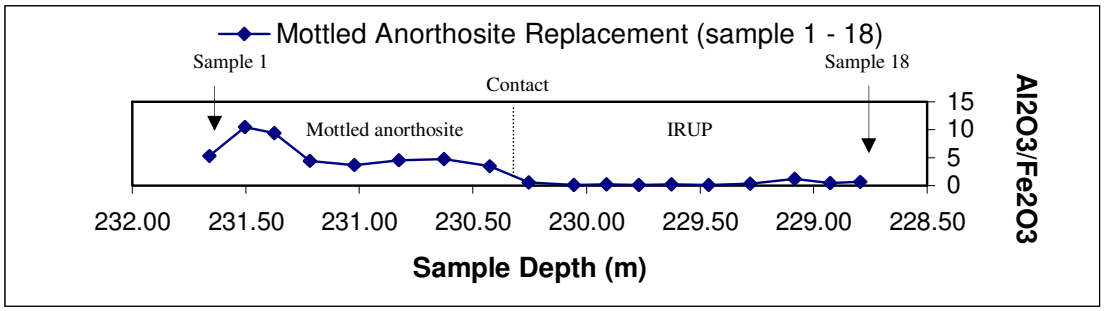

Figure 8.2a: The Al_2O_3/Fe_2O_3 ratios in sample set "MAR" where mottled anorthosite is replaced by IRUP.

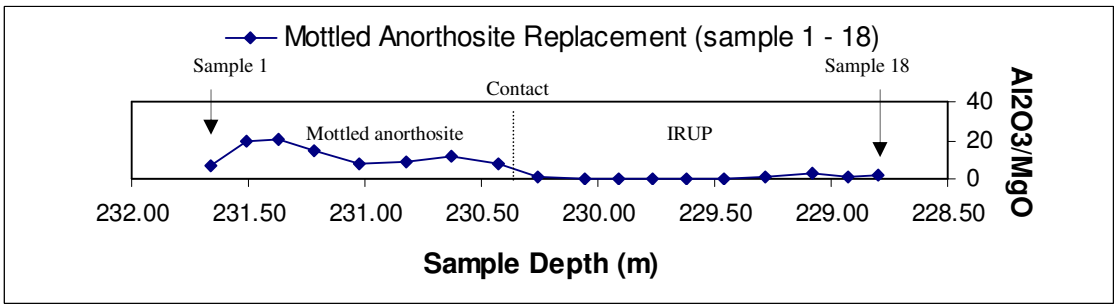

Figure 8.2b: The Al_2O_3/MgO ratios in sample set "MAR" where mottled anorthosite is replaced by IRUP.

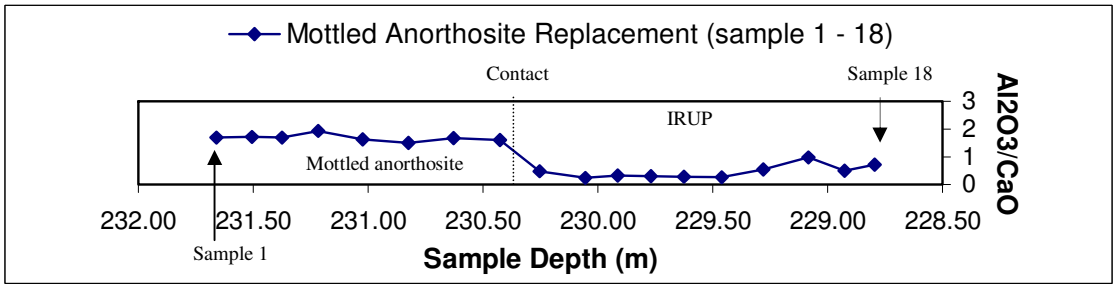

Figure 8.2c: The Al_2O_3/CaO ratios in sample set "MAR" where mottled anorthosite is replaced by IRUP.

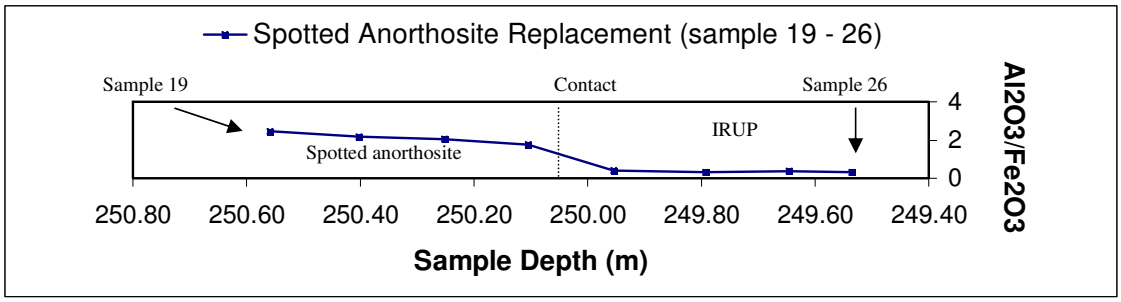

Figure 8.3a: The Al_2O_3/Fe_2O_3 ratios in sample set "SAR" where spotted anorthosite is replaced by IRUP.

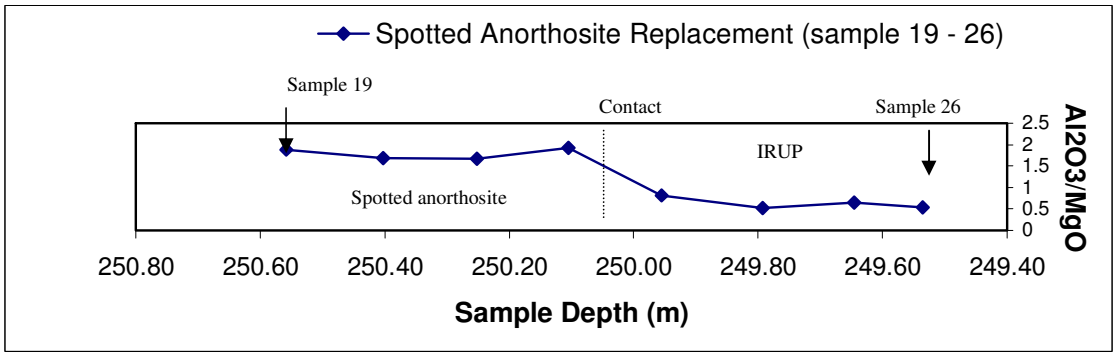

Figure 8.3b: The Al_2O_3/MgO ratios in sample set "SAR" where spotted anorthosite is replaced by IRUP.

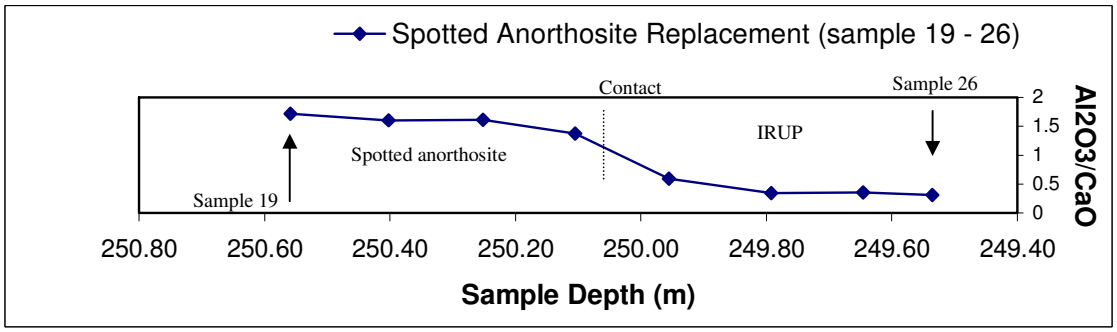

Figure 8.3c: The Al_2O_3/CaO ratios in sample set "SAR" where spotted anorthosite is replaced by IRUP.

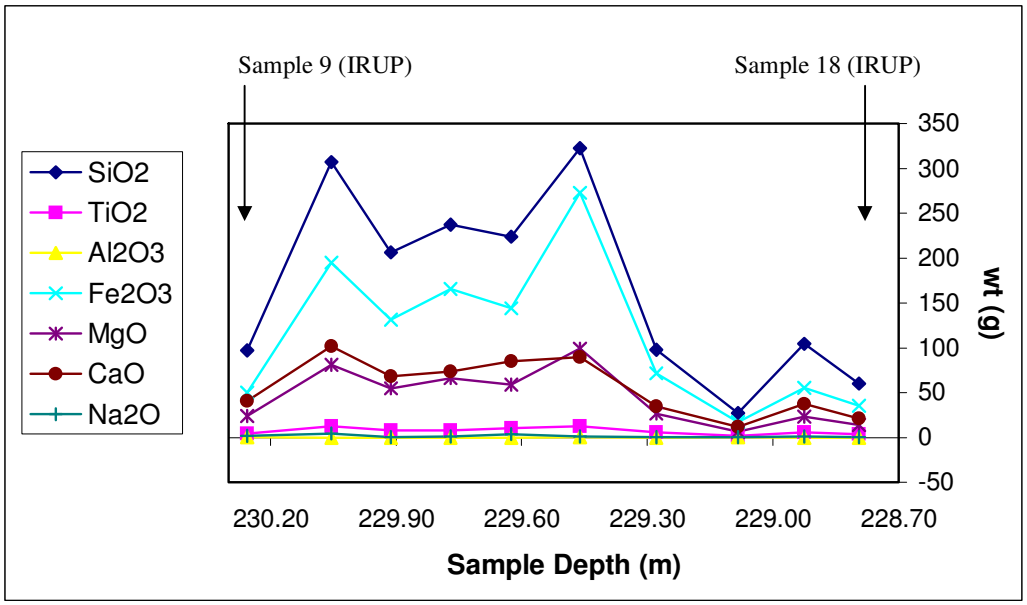

Figure 8.4a: Indicating the gains (in gram) of IRUP samples relative to the average composition of mottled anorthosite in sample set "MAR".

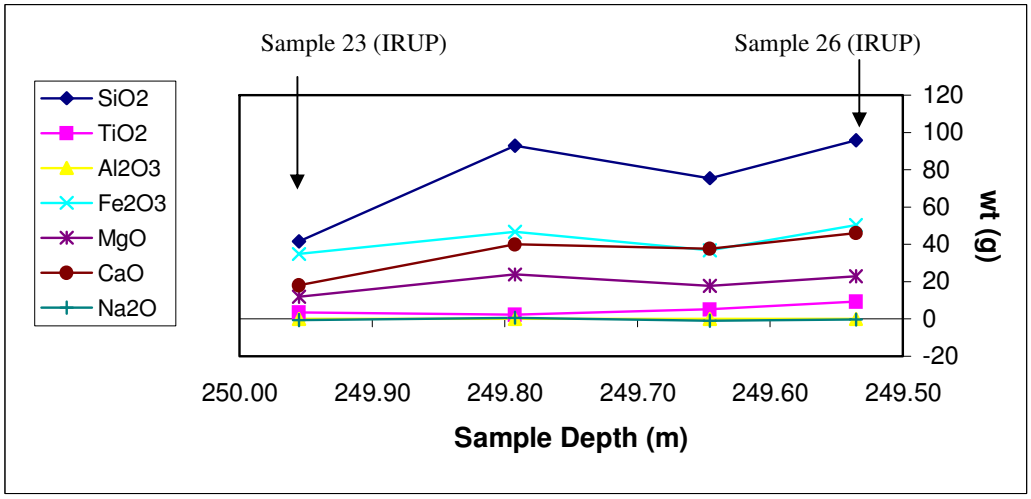

Figure 8.4b: Indicating the gains (in gram) of IRUP samples relative to the average composition of spotted anorthosite in sample set "SAR".

Geochemical Differences between IRUP Samples:

Comparison between Visually Different IRUPs:

Two visually different IRUPs were identified: a) a finer grained greenish variety, represented by sample 44 (at 446m drilling depth) and b) a coarser grained greyish variety, represented by sample 46 (at 665m drilling depth).

The geochemical data for the two varieties of IRUP were plotted on a X-Y chart for direct comparison (Fig 8.5), which indicates that the finer grained greenish variety of IRUP (higher in stratigraphic height) is relatively richer in Fe_2O_3, Na_2O, and Al_2O_3 relative to the coarser grained greyish variety of IRUP.

Figure 7.7a plots the geochemical data for sample 44 (the finer grained greenish variety of IRUP) against sample 43 (the host mottled anorthosite). The diagram shows that the IRUP of sample 44 is enriched in Fe_2O_3 and MgO relative to the host rock. Figure 7.7b plots the geochemical data for sample 46 (the coarser grained greyish variety of IRUP) against sample 45 (the host spotted anorthosite). The diagram shows that the IRUP of sample 46 is enriched in Fe_2O_3, MgO, and CaO compared relative to the host rock. It follows that there is an indication that the composition of IRUP may be related to the composition of the host cumulate rock it replaces.

Another possible explanation for the differences in IRUP compositions may be the potential presence of zones of varying composition within the Rooikoppies IRUP, following that different events of IRUP formation resulted in texturally and compositionally different IRUP.

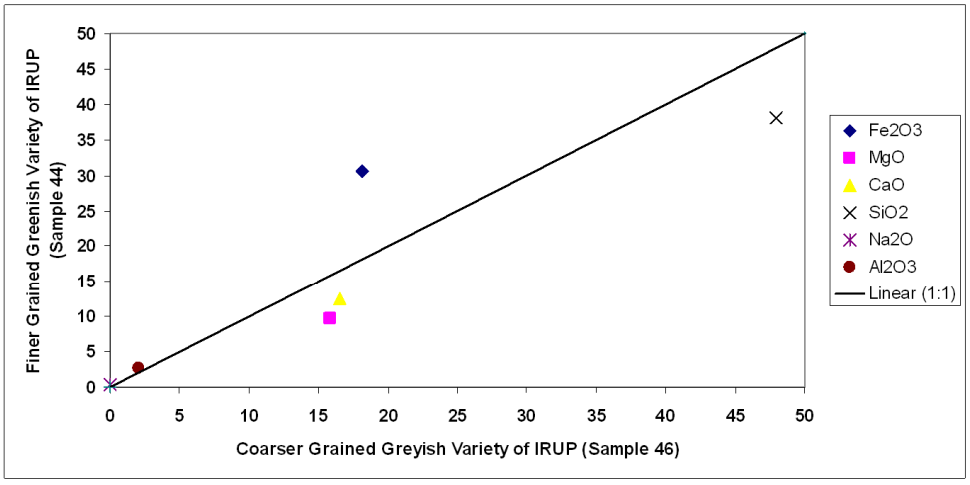

Figure 8.5: A direct comparison between the finer grained greenish variety of IRUP, sample 44 (at 446m drilling depth), and the relatively coarser grained greyish variety of IRUP, sample 46 (at 665m drilling depth).

IRUP Samples Above (where it replaces pyroxenite) and Below (where is replaces mottled anorthosite) the UG2 Chromitite Layer:

At the Karee mine the UG2 chromitite layer has a hanging wall pyroxenite and footwall anorthosite. The purpose of investigating samples directly above and below the UG2 chromitite was to establish whether or not the original cumulus composition of the host rocks affected the composition of post-cumulus IRUPs. Figure 7.13 generally shows that the IRUP samples closest to the UG2 chromitite layer (above and below) tends to be relatively depleted in silica, magnesium, and calcium, while being enriched in Fe_2O_3 relative to the IRUP samples farther from the UG2 chromitite. A trend is also indicated in the trace element chemistry, where the samples closest to the UG2 are relatively poorer in Cr and Ni. Figure 7.13 is, however, inconclusive as to whether or not there is a difference in the composition of IRUP above and below the UG2 chromitite layer.

IRUP at Variable Depths:

Viljoen and Scoon (1985) and Scoon and Mitchell (1994) suggested that the IRUP composition is related to height due to fractionation. Figure 7.16 is a graph indicating the geochemistry of selected IRUP samples at variable depths. The diagram indicates that, except for sample number 40, IRUP becomes relatively depleted in Fe_2O_3, and MgO, while becoming richer in CaO, Al_2O_3, Na_2O, and Ti_2O with increasing stratigraphic height. These geochemical changes are in contradiction with the expected trends for fractionation, which normally result in increased Fe_2O_3, and MgO contents with increased stratigraphic height.

The data in Figure 7.16 is also in contradiction with analyses of the two visually different varieties of IRUP (discussed in Chapter 8.2.1), which indicate that the IRUP at a higher stratigraphic level is richer in iron and magnesium (in accordance with normal fractionation patterns). A possible explanation for these inconsistencies may be the potential presence of zones of varying composition within the Rooikoppies IRUP. The evidence from his study is therefore inconclusive as to the hypothesis that IRUP composition is related to stratigraphic height due to fractionation.

Mineral Chemistry:

It was hypothesised that the mineral chemistry would reflect the progressive nature of the replacement process. The first notable feature of the mineral chemistry is that there are small changes in the composition of the minerals found in both the host cumulate rocks and the IRUP (i.e. plagioclase, olivine, and pyroxene). One exception is the composition of olivine, which shows a considerable increase in iron content from the unreplaced spotted and mottled anorthosite to the IRUP.

Variation in Feldspar Composition:

In sample set "MAR" most plagioclase analyses show very little compositional variation, except for a few analyses, which are poorer in calcium. It was established that these analyses were performed on plagioclase grains from thin section MAR 7L, which is located within IRUP material. As described in Chapter 7.7.1, these plagioclase grains are generally irregularly shaped inclusions of plagioclase in pyroxene, or plagioclase grains that are considerably smaller in size compared to the average grain size of plagioclase in IRUP. Figure 8.6 is a photograph of a plagioclase grain of which the composition does not plot in the average area of plagioclase composition. Whole rock chemical analyses indicated that the CaO wt % values remain approximately constant during the formation of IRUP in sample set "MAR". This was attributed to the combined effects of the addition of CaO, Fe_2O_3, and MgO in varying proportions. It is suggested that Ca-rich clinopyroxene formed around the already existing plagioclase grain, through a reaction whereby original cumulus orthopyroxene reacted with the IRUP forming fluid, enriched in CaO. An alternatively explanation may be that the growth of clinopyroxene took place at the outer margins of an originally smaller clinopyroxene grain due to the addition of CaO by the IRUP forming fluid, while clinopyroxene continued to grow inward at the inner margin (where it is in contact with the plagioclase inclusion) by using Ca and incorporating Al^* (occurring in quantities between 1 and 2% in clinopyroxene from thin section MAR 7L), from the inner plagioclase, thereby producing a more Na-rich irregularly-shaped plagioclase inclusion.

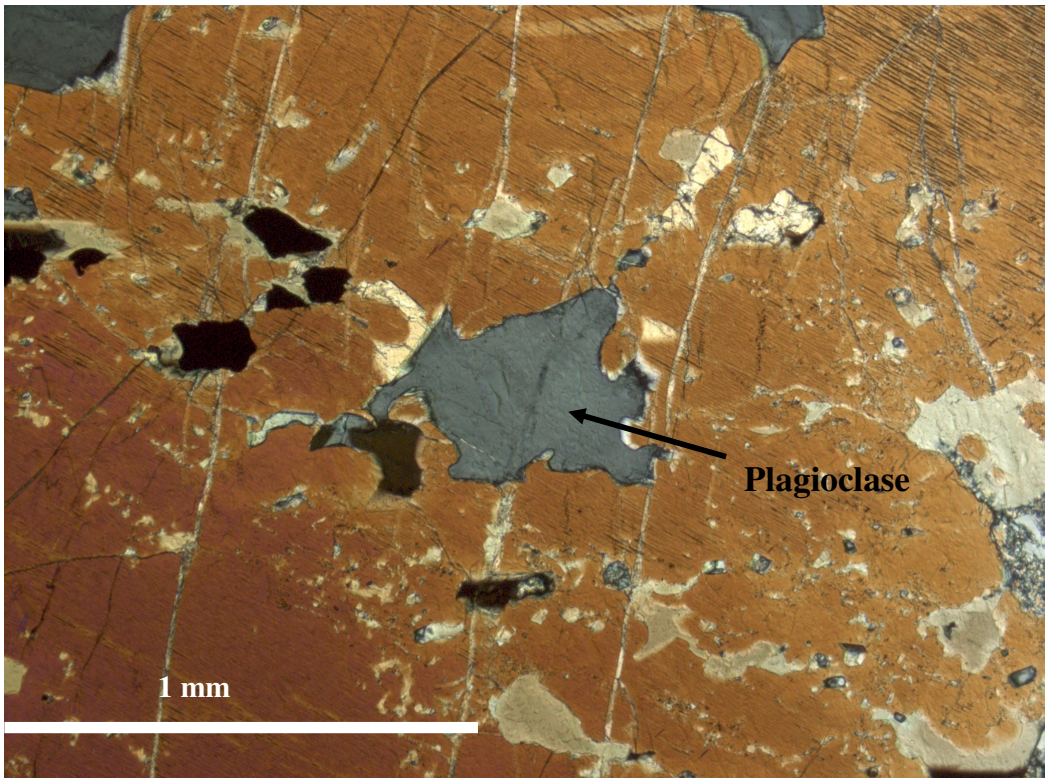

Figure 8.6: An inclusion of plagioclase in pyroxene from thin section MAR 7 L. The composition of this plagioclase grain does not plot in the area of average plagioclase composition.

Almost all thin sections in sample set "SAR" display very small variation in feldspar compositions, except for thin section SAR 4A (farthest from IRUP material), in which the plagioclase grains are poorer in the anorthite end-member and show some variation in plagioclase composition. It was determined that the more Na-rich plagioclase grains are relatively small compared to other plagioclase grains in the spotted anorthosite (Figure 8.7). The whole rock chemical analyses of sample set "SAR' indicated that there is an increase in the concentration of CaO. This was attributed to a larger proportion of CaO than Fe_2O_3 and MgO in the IRUP forming fluid. It is proposed that Ca was subsequently incorporated into both clinopyroxene and plagioclase, thereby producing relatively Ca rich plagioclase in the IRUP, compared to smaller more sodium-rich plagioclase grains in the spotted anorthosite.

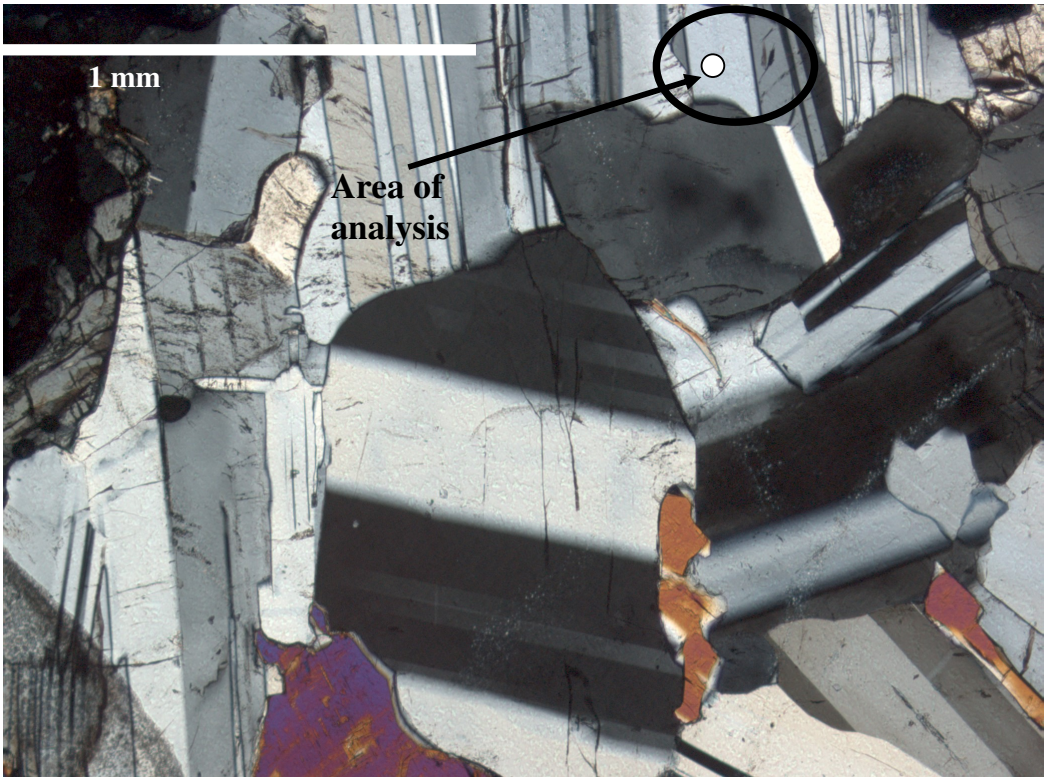

Figure 8.7: The relatively small, sodium rich plagioclase grain (analysed twice) is encircled. (Thin section SAR 4A).

Variation in Pyroxene Composition:

Figure 8.8 is a micrograph showing extremely fine exsolution lamellae of orthopyroxene in clinopyroxene. During further investigation of clinopyroxene using a scanning electron microscope, such exsolution lamellae become clearly visible. Figure 8.9 is a backscatter electron image of the clinopyroxene illustrated in Figure 8.8. The backscatter electron image shows the relatively brighter coloured exsolution lamellae of orthopyroxene within the darker clinopyroxene, and the two electron microprobe analytical points.

Analysis point number 69 incorporates more of the lighter coloured exsolution lamella and produced the following result: $Wo_{23.73}En_{45.02}Fs_{30.61}$.

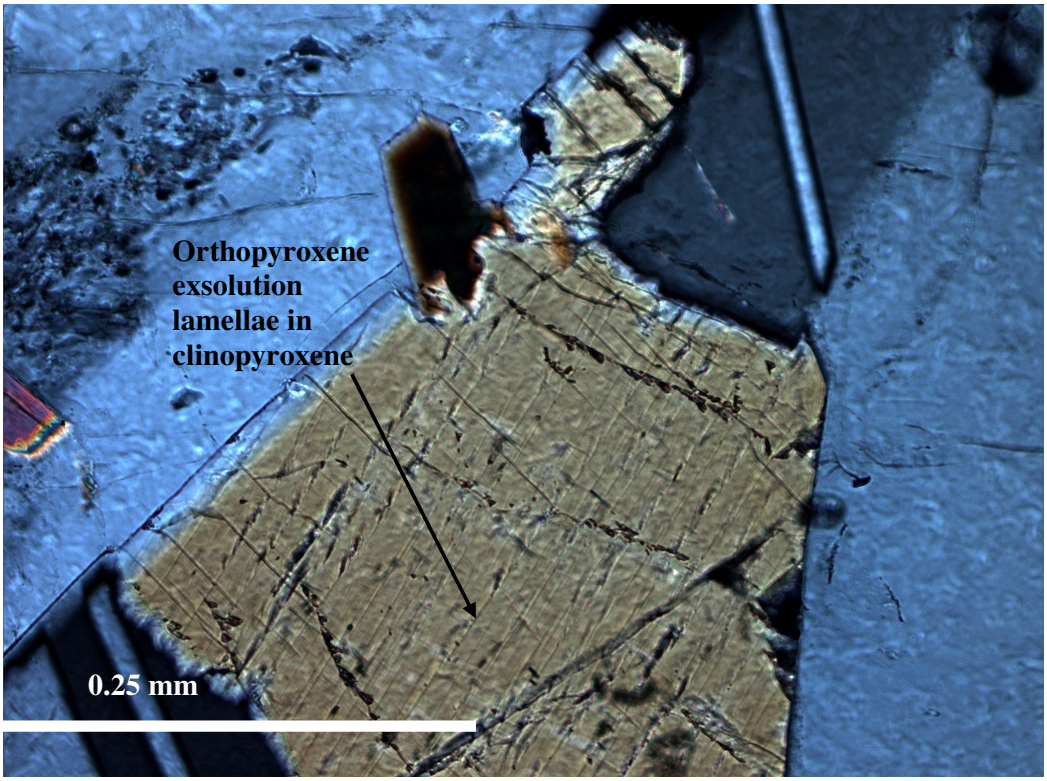

Figure 8.8: A clinopyroxene grain with extremely fine exsolution lamellae of orthopyroxene.

Conversely, analysis point number 70 incorporated relatively more of the darker host clinopyroxene and produced the following result: $Wo_{42.57}En_{38.30}Fs_{18.38}$. The variation of pyroxene composition within an individual thin section creates another point of interest. If one plots the compositions of these pyroxenes on a ternary diagram, it is noted that the mixed composition, between the clinopyroxene and associated orthopyroxene exsolution, does not lie in the area as predicted by the tie lines. Figure 8.10 is a ternary diagram indicating the stability fields of clinopyroxene and orthopyroxene with the standard tie lines (solid lines) radiating outward from the clinopyroxene field towards the corners of enstatite and ferrosilite (orthopyroxenes). Analyses numbers 69 and 70 are two analyses representing different proportions of pure compositions, which will be defined by the tie line (dashed line) that connects them. It is clear that the exsolution of orthopyroxene did not follow the standard orientation of tie lines, but deviated towards the ferrosilite corner. Such trends were also observed in data presented by Reid (2002), who did not provide any explanations as to the origin of these trends. It is suggested that a possible explanation may be that clinopyroxene has a lower closing temperature than orthopyroxene, but this would require further investigation for confirmation.

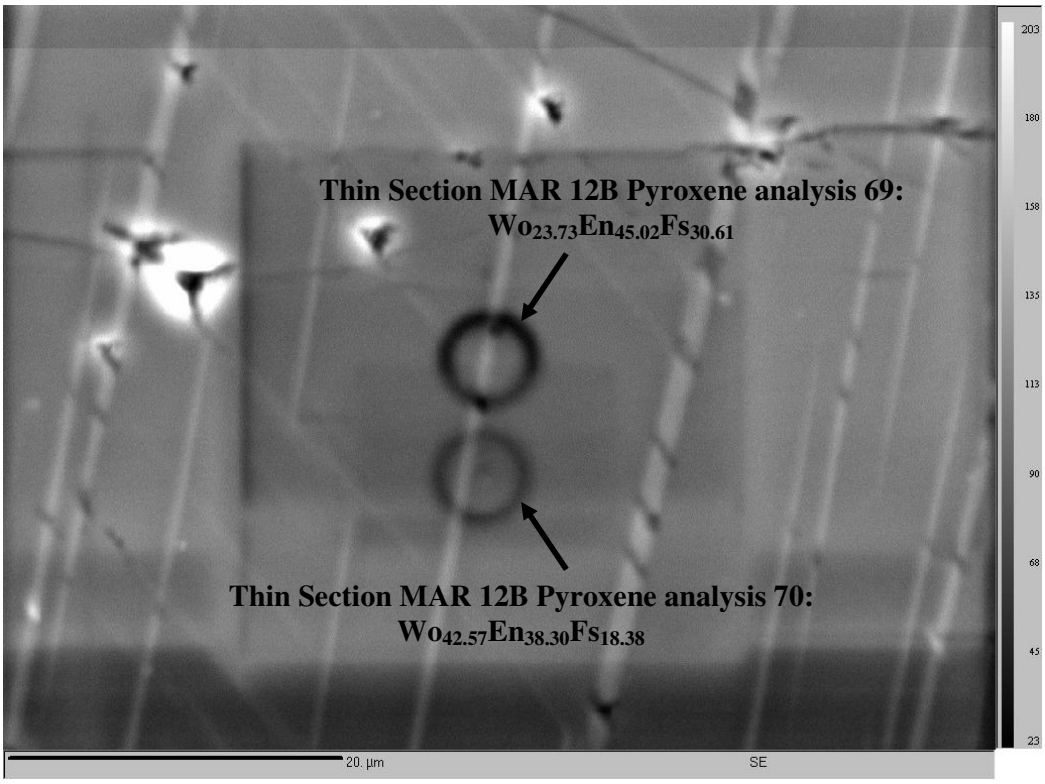

Figure 8.9: The backscatter electron image of lighter coloured orthopyroxene exsolution lamellae within darker clinopyroxene. The two black circles in the centre of the image are the electron microprobe analytical points.

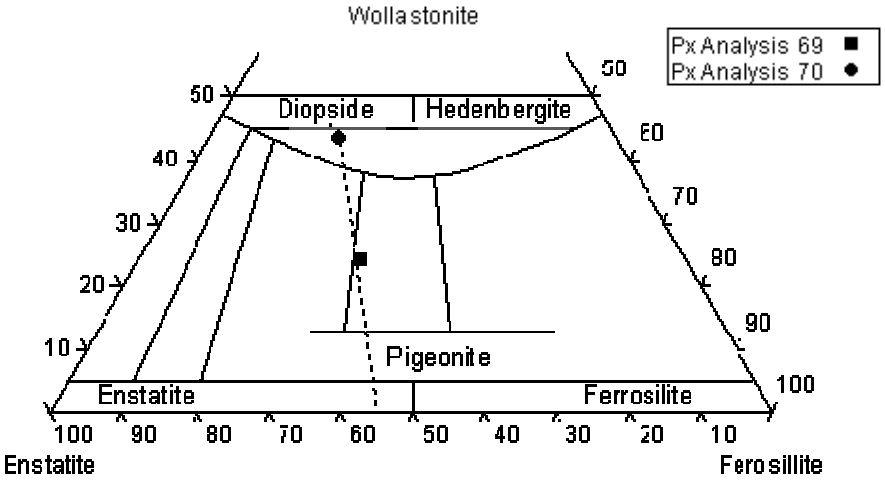

Figure 8.10: Two different composition of one pyroxene grain as a result of mixed electron microprobe analyses of clinopyroxene and exsolved orthopyroxene. The orthopyroxene exsolution deviates from the standard orientation of the tie lines towards the ferrosilite corner (overlay adapted from Klein and Hurlbut, 2000).

Variation in Olivine Composition:

Electron microprobe analyses of olivine revealed that only sample set "MAR" shows variation between the compositions of olivine found in IRUP and olivine found in the cumulate host rock, with IRUP olivine being more fayalitic compared to the host mottled anorthosite. Olivine, however, is not necessarily a major constituent of the spotted and mottled anorthosite host rocks. Schiffries (1982) attributed the formation of olivine in the dunitic Driekop pipe to the desilication of host rock orthopyroxene. The whole rock chemical data from this thesis indicate that the changes in silica content is within analytical reproducibility. Desilication is therefore not supported as an olivine forming process. It is proposed that olivine formed directly from the IRUP forming fluid, which, according to the geochemical data, was enriched in iron and magnesium, and slightly silica poor.

Results also indicate that there is very little variation in the composition of olivine within the IRUP material.

Lamellar Exsolution Features in Olivine:

Wager (1929) described hortonolite that "encloses minute tabular interpositions arranged in irregular plates". These "tabular interpositions" appear to be fairly common in olivine associated with ultramafic pegmatite, being described in both iron rich ultramafic pegmatite and the magnesium rich varieties from different localities. Schiffries (1982) studied olivine with oriented inclusions of magnetite consisting of "closely spaced flat needles", reported to be similar to the "tabular interpositions" described by Wagner (1929). Scoon (1987) described "dendrite-like intergrowths of an opaque oxide" in pegmatite olivine (apparently not found in cumulus Bushveld olivines) from his study at the Amandelbult Section mine. Reid and Basson (2002) identified olivine that contains "submicron needle and platelet exsolution of Fe-oxide". Similar exsolution lamellae of magnetite were described in thin sections from the Rooikoppies IRUP body in this thesis (Chapter 5).

Putnis (1979) studied lamellar exsolutions in olivine using the electron microscope and concluded that they formed as a result of the oxidation of olivine. The oxidation process is said to produce an "oxidized olivine structure", which subsequently decomposes to a linear plate-like intergrowth of magnetite and pyroxene in the olivine. Moseley (1984) described such exsolution features in olivine as the symplectic intergrowth between magnetite and pyroxene. He proposed that the olivine structure might contain ferric iron at elevated temperatures. The structure contracts upon cooling until electrostatic stability between Fe^{3+} and Si^{4+} cannot be maintained and Fe^{3+} is exsolved in the form of magnetite. Moseley (1984) proposed the following equation for the reaction:

$$3Fe^{3+}_{4/3} + Fe^{2+}_{2}SiO_4 + 4X_2SiO_4 \longrightarrow 2Fe_3O_4 + 4X_2Si_2O_6$$

where X = Ca, Mg, and Fe. The author further suggested that pyroxene incorporates elements that are incompatible into the olivine structure, such as Al and Ca.

Zhang et al. (1999) described oriented magnetite lamellae in olivine of the Dabie ultra-high (UHP) ultramafic rocks in central China. The authors proposed four hypotheses for their occurrence: a) the oxidation of olivine, b) the decomposition of Fe^{3+} bearing olivine formed at >6 GPa, c) the exsolution of a spinel (wadsleyite) solid solution Fe_3O_4 - $(Fe,Mg)_2SiO_4$ during decompression, and d) the breakdown of phase $A[Mg_7Si_2(OH)_6]$ + enstatite.

Considering the geological environment, with hydrous solutions migrating through cumulus rocks, it is proposed that IRUP olivine incorporated unknown quantities of Fe^{3+} in its structure, which subsequently exsolved as an intergrowth between magnetite and pyroxene upon cooling.

Genetic Models:

Several suggestions have been made to explain the origin of IRUP in the BIC, of which the hypothesis that it was formed by replacement processes as a result of fluid/aqueous solutions seems to carry the most support.

Wagner (1929) suggested that the dunitic bodies formed by the intrusion of dunitic rest magma remaining after the differentiation processes responsible for the formation of the Critical Zone. Wagner (1929) proposed that the rest magma differentiated upon cooling and subsequently separated into a) iron-rich, magnesia-poor and b) iron-poor, magnesia-rich fractions, which were ultimately responsible for the formation of the pegmatitic bodies.

Cameron and Desborough (1964) explain such pegmatite bodies as products of replacement processes induced by high temperature fluids acting as a transport medium. They continue to mention that all the components necessary to produce the current pegmatite composition are available from the Critical Zone rocks through which the fluids would have migrated.

Through his interpretation of the mineral chemistry of amphibole and serpentine, which have anomalously high chlorine contents, and the formation of platinum group minerals, oxides and sulphides, Schiffries (1982) suggested that the Driekop pipe formed through infiltration metasomatism by a chloride solution. Schiffries (1982) proposed that olivine was produced by the desilication of orthopyroxene and that the dissolution of plagioclase also contributed to the changes in bulk composition of the host rock. Schiffries (1982) calculated a net volume loss of 67% during the formation of the Driekop pipe. The mineral reactions responsible for the formation of the pipe and volume loss could ultimately be responsible for the significant structural collapse of the Critical Zone cumulate rocks surrounding the Driekop pipe.

Stumpfl and Rucklidge (1982) proposed that the upward migration of iron-rich fluids were structurally controlled and that these fluids were responsible for the formation of dunite pipes due to metasomatism of the host rocks.

Tegner and Wilson (1994) studied a relatively magnesian dunite-clinopyroxenite pegmatoidal pipe, with an olivine rich core, surrounded by a clinopyroxenitic outer shell (on the farm Tweefontein), where it replaces upper Critical Zone cumulate rocks. They suggest that the transformation from leuconorite (85% plagioclase, 10% orthopyroxene, 5% clinopyroxene) to clinopyroxenite (the outer shell of the body – 85% clinopyroxene, 10% orthopyroxene, 5% plagioclase) by a migrating fluid requires substantial addition of MgO, FeO and CaO, together with the removal of Al_2O_3 and Na_2O in a continuously flushed open system. The authors propose that the magnesian core of the Tweefontein pipe formed by the influx of an olivine-saturated magma that intruded from below (magma derived from higher stratigraphic levels would probably not have contained magnesian olivine). The clinopyroxenitic shell is believed to have formed by subsequent assimilation of plagioclase and the host leuconorite.

Viljoen and Scoon (1985) proposed that IRUP represents the residual intercumulus fluid generated by fractional crystallization during the development of cyclic units in the upper Critical Zone. It is further postulated that IRUP either developed by the metasomatic replacement of cumulus rock or by the direct crystallization from pegmatitic fluid.

Scoon (1987) analysed several olivine grains in thin sections containing IRUP, harzburgite cumulate, and the contact zone between the two. He interpreted the data to represent a straight-line relationship between cumulus olivine and pegmatitic olivine, with olivine in the contact zone having an intermediate composition. The straight-line relationship between cumulus, intermediate and pegmatitic olivine is believed to be the result of different exposure times to the pegmatitic liquid. The concluding remarks by the author are that pegmatitic olivines formed by the metasomatic replacement of already existing cumulus olivines and not by the metasomatism of other phases.

The harzburgitic cumulates (“pseudoreefs”) are separated by leuconorite and anorthosite layers, which, according to Scoon (1987), commonly host ultramafic pegmatite, while harzburgite layers remain unaltered. This agrees with the findings of Wagner (1929), Schiffries (1982), Scoon and Mitchell (1994), and Viljoen and Scoon (1985) that the ultramafic pegmatite preferentially replaces the more felsic (anorthositic) cumulates. However, Tegner et al. (1994) found that the more mafic leuconorite was more easily replaced than the typical leuconorite.

Wager and Brown (1968) and Jaupart et al. (1984) proposed the existence of residual liquid (“rejected melt that ponds at the crystal-liquid interface”) in layered intrusions. Scoon and Mitchell (1994) expect such liquids to be rich in iron and, due to their higher density, would drain downward into “a partially crystalline mush” and blend with intercumulus liquid in anorthositic layers.

Reid and Basson (2002) feel that their observations support an origin by means of replacement. Field data however, create difficulty in explaining the physical

mechanism of IRUP formation. Reid and Basson (2002) observed that some IRUP spread laterally beneath the Merensky chromitite layer – arguing for the upward migration of iron-rich fluid under the driving force of either hydrostatic overpressure or volatile expansion. In contrast, an IRUP vein was described to terminate from above against an anorthosite layer, which requires replacement of host cumulate rock from above. Clinopyroxene is described with local "patchy replacement" by brown amphibole and biotite.

Based on Sr isotope data, Reid and Basson (2002) conclude "IRUP parent melt" was probably derived from Upper Zone magmas. The occurrence of IRUP at Northam and the field evidence for upward migration of "IRUP parent melt" is clarified with reference to the so-called gap areas in the Rustenburg Layered Suite, where Upper Zone cumulates are in lateral contact with the upper Critical Zone. This relationship would allow for "IRUP parent melt", with Upper Zone geochemical signatures, to migrate laterally, upward and possibly downward into the adjacent upper Critical Zone, thereby generating the current field relationships to upper Critical Zone cumulate layers.

Braun et al. (1994) interpreted pegmatoids beneath the J-M Reef, in the Stillwater Complex, to represent channel-ways, through which fluids migrated, with subsequent recrystallization/replacement of the host rocks. Owing to the more evolved nature of the pegmatoid, the authors believe that the "pegmatoid-forming fluids evolved late in the crystallization of intercumulus silicate liquid".

McBirney and Sonnenthal (1990) studied replacement attributed to metasomatic processes in the Skærgard Intrusion, east Greenland. The metasomatism resulted in two contrasting felsic and mafic rock types, of which the mafic rock is described as an olivine clinopyroxenite. McBirney and Sonnenthal (1990) ascribed the alteration of the modal proportions and, in some cases, the mineral chemistry of gabbro-norites, to metasomatic changes due to high temperature reactive fluids moving through the rocks.

Whether or not the pegmatoids in the Bushveld Complex, the Stillwater Complex, and the Skærgard Intrusion are of the same or of different composition, all these igneous complexes contain components indicating possible pervasive fluid activity. The frequent occurrence of ultramafic pegmatite in the Bushveld and other igneous complexes suggest that the development of pegmatites may be an integral part of the formation of large layered intrusions, an idea supported by most authors on the subject.

The theories on the genesis of IRUP bodies in large layered intrusions and how they relate to observations made for the Rooikoppies IRUP body is summarized in Table 8.1.

Table 8.1: A summary of genetic models for IRUP formation and how they relate to observations made for the Rooikoppies IRUP body.

Author/s	Observation/ Suggested Process	Related observation for the Rooikoppies IRUP body	Interpretation Valid for the Rooikoppies IRUP body?
Wagner, 1929	Intrusion of dunitic rest magma.	The mineralogy partially agrees with the crystallization of a dunitic magma with the presence of olivine.	The large proportion of clinopyroxene and presence of plagioclase suggest that the fluid responsible for the formation of the Rooikoppies IRUP body was not a dunitic magma.
Cameron and Desborough, 1964	Replacement processes induced by high temperature fluids acting as a transport medium.	Plagioclase is interpreted as being original cumulate plagioclase surrounded/enclosed by large crystals of olivine and clinopyroxene.	The Rooikoppies IRUP body is interpreted to have been formed as a result of high temperature fluids, rich in Fe and Mg, pervasively infiltrating cumulate host rock, before replacing and diluting the original cumulate phases (predominantly plagioclase and pyroxene).
Schiffries, 1982	Infiltration metasomatism by a chloride solution (an interpretation of chlorine in amphibole and serpentine)	The Rooikoppies IRUP only contains Amphibole as a patchy alteration product of clinopyroxene. Amphiboles were found not to contain any chlorine.	Amphibole compositions suggest that the fluid responsible for the formation of the Rooikoppies IRUP body was probably not enriched in chlorine.
Stumpfl and Rucklidge, 1982	The upward migration of iron-rich fluids were structurally controlled and that these fluids were responsible for the formation of dunite pipes due to metasomatism of the host rocks	Data from the investigation of open pit mining operations indicate the presence of IRUP along joints and fractures.	The Rooikoppies IRUP body may have been formed as a result of IRUP forming fluid infiltrating host cumulate rocks via structural inconsistencies such as joints and faults.
Tegner and Wilson, 1994	The authors studied a relatively magnesian dunite-	Even though potential zones of varying chemical composition was	Data from this study suggests that the Rooikoppies IRUP body did not form through the influx of an olivine-

	clinopyroxenite pegmatoidal pipe, with an olivine rich core (formed by the influx of an olivine-saturated magma), surrounded by a clinopyroxenitic outer shell (formed by subsequent assimilation of plagioclase and the host leuconorite).	observed in some geochemical profiles along sections of drill core, an olivine-rich core and clinopyroxenitic shell was not identified in the Rooikoppies IRUP body.	saturated magma and subsequent processing resulting in a pyroxenitic shell, but that there may have been multiple replacement events, resulting in zones of variable chemical composition.
Viljoen and Scoon, 1985	The authors postulated that IRUP either develops by the metasomatic replacement of cumulus rock or by the direct crystallization from pegmatitic fluid.	The Rooikoppies IRUP body was observed to contain plagioclase inclusions in clinopyroxene. It is suggested that these plagioclase grains represent original cumulus plagioclase around which original cumulus orthopyroxene reacted with IRUP-forming fluid to form clinopyroxene.	Both processes suggested by Viljoen and Scoon, 1985, may hold true for the Rooikoppies IRUP body, whereby cumulus pyroxene reacted with IRUP forming fluid to produce clinopyroxene, and olivine and additional clinopyroxene crystallized directly from the Fe, Mg, and Ca-rich IRUP-forming fluid.
Scoon, 1987	The author concluded that pegmatitic olivines formed by the metasomatic replacement of already existing cumulus olivines and not by the metasomatism of other phases (interpreted from a straight line relationship between the compositions of cumulus and IRUP olivine).	Data from this study indicates that IRUP olivine is enriched in Fe compared to minor olivine from the host anorthosite (sample set “MAR”).	It is possible that a certain proportion of IRUP olivine formed through the metasomatic interaction between cumulus olivine and the IRUP-forming fluid. It is however suggested that a larger proportion of IRUP olivine crystallized directly from the IRUP-forming fluid.

Scoon and Mitchell, 1994	The authors expect residual liquids to be rich in iron and, due to their higher density, to drain downward into "a partially crystalline mush" and blend with intercumulus liquid in anorthositic layers.	No observations during this study can confirm the interpretation that residual melts drain downward through critical zone anorthositic crystal mushes to produce discordant IRUP bodies.	Data produced during this study have not been used to test this theory of genesis.
Reid and Basson, 2002	Observations support an origin by means of replacement. Clinopyroxene is described with local "patchy replacement" by brown amphibole and biotite.	Clinopyroxene was observed to contain what was described as "patchy alteration to amphibole".	It is suggested that similar replacement processes occurred during the formation of the Rooikoppies IRUP body as did during the formation of the IRUP body at Northam.

Conclusion:

The Rooikoppies pegmatite, consisting essentially of clinopyroxene, olivine, and plagioclase, with magnetite and ilmenite as accessory phases, is classified as a "silicate rich variety" of IRUP according to the classification scheme developed by Viljoen and Scoon, 1985. Investigation of drill cores revealed two, visually and geochemically different, varieties of IRUP: a) a fine grained greenish variety, and b) a coarse grained greyish variety of IRUP. The geochemical profile of sample set "MAR", indicated towards an area within the IRUP material with noticeably higher proportions of Fe_2O_3 and MgO, compared to other IRUP samples from sample set "MAR". From the investigation of element ratios and the relative mobility of elements, it was concluded that aluminium acted as an immobile element. Gresens' equations for metasomatic alteration, indicated that IRUP with the maximum change relative to the host rock had increased in net weight by a factor of 3.04 (calculation based on sample set "SAR" using equation 2 from Chapter 8.1).

It is concluded that the Rooikoppies IRUP formed through the pervasive infiltration of a fluid significantly enriched in iron, magnesium, calcium, and titanium. The addition of these elements to the already existing cumulate rocks caused dilution of feldspar (which generally does not change in composition from the host rocks to the IRUP), and the crystallization of large amounts of clinopyroxene and olivine. Considering the presence of two visually and chemically different varieties of IRUP and the fact that some IRUP samples appear to be more enriched in Fe_2O_3 and MgO compared to others, it is suggested that the formation of the Rooikoppies IRUP is not restricted to a single event, but rather that the IRUP body formed through multiple replacement events, resulting in a network of chemically different zones within one large IRUP body.

It is proposed that subsequent studies focus on the influence of the composition of the host cumulate rock on the IRUP and whether the geochemically distinct IRUP zones are a result of different fluid composition, or a function of the host rock geochemistry. Further electron microprobe analyses are required to obtain sufficient data for geothermometry studies, which may provide a better understanding of the nature of the fluids responsible for IRUP formation. This thesis suggests that there may be some structural controls on IRUP formation; it follows that further studies could focus on the relationship between the geotectonic history and IRUP formation in the Bushveld Igneous Complex.

References:

Braun, K., Muerer, W., Boudreau, A.E. and McCallum I.S. (1994). Compositions of pegmatoids beneath the J-M Reef of the Stillwater Complex, Montana, USA. *Chemical Geology*, **113**, 245-257.

Cameron, E.N., Desborough, G.A. (1964). Origin of certain magnetite-bearing pegmatites in the eastern part of the Bushveld Complex, South Africa. *Economic Geology*, **59**, no. 2, 197-225.

Cawthorn, R.G. (1995). A re-evaluation of the magma compositions and processes in the upper Critical Zone of the Bushveld Complex. *Economic Geology Research Unit*, 286.

Cawthorn, R.G., and Poulton, K.L., (1988). Evidence for fluid in the footwall beneath potholes in the Merensky Reef of the Bushveld Complex. *In: Geo-Platinum 87.* Pritchard, H.M., Potts, P.J., Bowles, J.F.W. and Cribb, S.J. (eds.). Elsevier, London, 343-356.

Eales, H.V., and Cawthorn, R.G., (1996). The Bushveld Complex. In: Cawthorn, R.G. (Ed.), *Layered Intrusions*, Elsevier, Amsterdam, 181-230.

Eales, H.V., Marsh, J.S., Mitchell, A.A., De Klerk, W.J., Kruger, F.J., and Field, M., (1986). Some geochemical constraints on models for the crystallization of the upper Critical Zone – Main Zone interval, north-western Bushveld Complex. *Mineralogical Magazine*, **50,** 567-582.

Gresens, R.L. (1967). Composition-volume relationships of metasomatism. *Chemical Geology*, **2**, 47-65.

Jaupart, C., Brandeis, G., and Allegre, C.J. (1984). Stagnant layers at the bottom of convecting magma chambers. *Nature*, **308**, 535-538.

Kaiser, H. and Specker, H. (1956). Bewertung und Vergleich von Analysenverfahren. *Zeitschrift für Analytische Chemie,* **149**, 46-66.

Klein, C. and Hurlbut, C.S., Jnr. (2000). *Manual of mineralogy*, Revised 21st edition, John Wiley and Sons, Inc. New York / Chichester / Weiheim / Brisbane / Singapore / Toronto.

Kruger, F.J. (1994). The Sr-isotopic stratigraphy of the western Bushveld Complex. *South African Journal of Geology*, **97**, 393-398.

McBirney, A.R. and Sonnenthal, E.L. (1990). Metasomatic replacement in the Skærgard Intrusion, east Greenland: Preliminary observations. *Chemical Geology*, **88**, 245-260.

Moseley, D. (1984). Symplectic exsolution in olivine. *American Mineralogist*, **69**, 139-153.

Peyerl, W. (1982). The influence of the Driekop dunite pipe on the Platinum-group mineralogy of the UG-2 chromitite in its vicinity. *Economic Geology*, **77**, 1432-1438.

Putnis, A. (1979). Electron petrography of high-temperature oxidation in olivine from the Rhum Layered Intrusion. *Mineralogical Magazine*, **43**, 293-6.

Reid, D.L. and Basson, I.J. (2002). Iron-rich ultramafic pegmatite replacement bodies within the Upper Critical Zone, Rustenburg Layered Suite, Northam Platinum Mine, South Africa. *Mineralogical Magazine*, **66**, no. 6, 895-914.

Schiffries, C.M. (1982). The petrogenesis of a platiniferous dunite pipe in the Bushveld Complex: Infiltration metasomatism by a chloride solution. *Economic Geology*, **77**, 1439-1453.

Schurmann, L.W. and Von Gruenewaldt, G. (1991). The petrogenesis of the upper Critical Zone in the Boshoek Section of the western Bushveld Complex. *Institute for Geological Research on the Bushveld Complex*, 94.

Scoon, R.N. (1987). Metasomatism of cumulus magnesian olivine by iron-rich postcumulus liquids in the upper Critical Zone of the Bushveld Complex. *Mineralogical Magazine*, **51**, 389-96.

Scoon, R.N. and Mitchell, A.A. (1994). Discordant Iron-Rich Ultramafic Pegmatites in the Bushveld Complex and their relationship to Iron-Rich Intercumulus and Residual Liquids. *Journal of Petrology*, **35**, 881-917.

Simon, J.L. and Bruce, P. (1991). Resampling: a tool for everyday statistical work. Chance **4,** 22-32.

Simon, J.L. (1997). Resampling: The "New Statistics". 2nd edition. Resampling Stats Inc., Arlington, VA, 436.

Stumpfl, E.F. and Rucklidge, J.C. (1982). The platiniferous dunite pipes of the eastern Bushveld. *Economic Geology*, **77**, 1419-1431.

Tegner, C., Wilson, J.R. and Cawthorn, R.G. (1994). The dunite-clinopyroxenite pegmatoidal pipe, Tweefontein, eastern Bushveld Complex, South Africa. *South African Journal of Geology*, **97**, no. 4, 415-430.

Viljoen, M.J. and Scoon, R.N. (1985). The distribution and main geologic features of discordant bodies of iron-rich ultramafic pegmatite in the Bushveld Complex. *Economic Geology*, **80**, 1109-1128.

Von Gruenewaldt, G. (1973). The main and upper zones of the Bushveld Complex in the Roossenekal area, Eastern Transvaal. *Economic Geology*, **76**, 207-227.

Wager, L.R., and Brown, G.M. (1968). *Layered Igneous Rocks*. London: Oliver Boyd, 588.

Wagner, P.A. (1929). The platinum deposits and mines of South Africa. *C. Struik*, Cape Town, 50.

Wilson, M.G.C., and Anauesser, C.R. (1998). *The Mineral Resources of South Africa*. The Council for Geoscience, South Africa, 532-568.